Simulating fluid flow surrounding carbonate fault zone

Adrian Øwre Ryvoll

Master Thesis in Geosciences

Structural Geology and Tectonics

60 credits

Department of Geosciences

Faculty of Mathematics and Natural Sciences

UNIVERSITY OF OSLO

August 2022

Simulating fluid flow surrounding carbonate fault zones

Supervisors: Dr. Emma Michie Haines (University of Oslo)

Co-supervisor: Professor Anita Torabi (University of Oslo) and associate professor Carlos Duque Calvache (University of Aarhus)

http://www.duo.uio.no/

Printed: Reprosentralen, Universitetet i Oslo

Abstract

De-risking of CO_2-storage sites is crucial for assessing its viability. The Alpha Prospect is reliant on faults in the carbonate-rich Cromer Knoll Formation acting as a seal to prevent CO_2 from leaking. However, prediction of carbonate fault permeability has not been researched enough for us to safely assume that these faults act as barriers. Hence, the well exposed carbonate faults on the island of Malta and Gozo were utilised to strengthen our understanding of permeability prediction in carbonate sequences.

To increase our understanding, a geocellular model of the Maltese Islands was created and populated using data for previously conducted field studies. Here, 23 faults with various attributes were modelled. In this thesis the main focus was on the two faults Il-Maghlaq Fault and the Victoria Line Fault. in addition, three other faults were compared to these main faults. Afterward, results from this modelling were implemented into a hydrogeological model, which was compared with observed well data.

The result implied that it is possible to predict which faults is sealing and which are not by examining the shale smear factor. Our preliminary assessment suggests that a SSF ≤ 5 is likely to produce a continuous shale smear for faults with large throw. The hydrogeological model showed the importance of having a continuous fault rock along the entire fault zone. The model with a thinned fault zone showed clear signs of leakage, while the model with the continuous fault rock show results similar to what is observed on the islands.

Acknowledgment

I want to express my gratitude toward all involved in my master's thesis. A special thanks to my supervisor Dr. Emma Michie Haines for her guidance within carbonate faults, teaching me T7, and critical assessment of various drafts. I also want to thank the co-supervisor Carlos Duque Calvache for his guidance within groundwater modelling. Lastly, I would like to thank Professor Anita Torabi for her critical assessment of my various drafts.

Preface

This master's thesis (ECTS 60) is submitted to the Department of Geosciences, University of Oslo (UiO), in the candidacy of the Master of Science in Geosciences (ECTS 120) following the Structural Geology and Tectonics program. The main supervisor of the thesis is Dr. Emma Michie Heines and the co-supervisors are associate professor Carlos Duque Calvache and Professor Anita Torabi.

This will contribute to methods for de-risking of CO_2 storage in the FRISK project, a spin-off project from NCCS task 9. Well data was provided by the Maltese Water and Energy Agency. Software is in the courtesy of Badleys (T7) and Aquavero (GMS)

Table of Content

List of figures

1 Introduction

1.1 Background and motivation

It is well known that faults can act as a barrier, a conduit, or a combination of both on fluids in the subsurface (Caine et al., 1996; Fisher & Knipe, 1998). While membrane sealing faults have proven to be predictable within siliciclastic sequences, it is yet to be fully understand in carbonates due to its unique deformation style and inherent heterogeneity (Agosta et al., 2007; Michie et al., 2021). Understanding how carbonates deform in fault zones is important for de-risking of Carbon Capture and Storage (CCS), which is a crucial contribution towards reaching the 2 degrees goal from the Paris agreement. Specifically, it is critical that any trap bounded by faults is sealing, with no possibility of CO2 to leak after injection to prevent contamination of overlying freshwater aquifers (Little & Jackson, 2010; Zheng et al., 2009). Hence, the purpose of this thesis is to address the difficulty and attempt to improve predictability of membrane seal behaviour of faults containing carbonates. This contribution aid with the assessment of several potential CO2 storage sites and reducing uncertainty, such as the alpha prospect of the Smeaheia CO_2 storage site within the Horda platform. This is a storage site which is bound by a large half-graben fault that offsets siliciclastic sequences containing carbonate layers.

Jurassic-Cretaceous formations within the tilted Smeaheia Fault Block are identified as a possible host to a potential CO_2 storage site (Mulrooney et al., 2020). Injecting CO_2 into the subsurface poses some risks, as fault zones are complex structures with potential leakage points. This means that faults should be mapped with care. An uncertainty within the Smeaheia Fault Block is the carbonate-rich Cretaceous interval where siliciclastic-based algorithms such as the shale gouge ratio does not apply (Mulrooney et al., 2020). To de-risk the injection of CO_2, it is key to improve our understanding of how marls may act as baffles or barriers in this case study.

One of the fault blocks located on the easternmost part of the Horda Platform is the Smeaheia Fault Block. This is a 15 km wide fault block bounded by the two N-S striking first order faults called the Vette Fault Zone and the Øygaarden Fault Complex (Lauritsen et al., 2018; Mulrooney et al., 2020) which has been identified as a possible CO_2 storage site. Here the

Fensfjord and Sognefjord Formation form the Viking Group has been identified as potential storage formations for CO_2-injectinon. The clay-rich mudstone of Draupne Formation is normally the most important caprock in the North Sea (Gabrielsen et al., 2020) and is also identified as the primary caprock in the Smeaheia Site. However, the Draupne Fm is observed to be severely thinned caused by erosion and potentially not sealing above the alpha prospect (Mulrooney et al., 2020). Eroded areas are reliant on a secondary seal, this has been observed in the Troll field where clay-rich sequences within the Cromer Knoll Groupe act as a caprock. Furthermore, it has been an increased focus on whether or not the carbonaceous sequences also can give sealing properties when faulted. However, it is yet to fully the behaviour of faulted sequences of carbonates.

1.2 Aim and objectives

The aim of this thesis is to calibrate any previously established or new relationships to predict fault rock permeability in carbonate sequences. Specifically, I will assess the ability to predict fault seal potential related to marl smearing. This will contribute to methods for de-risking of CO_2 storage in the FRISK project, a spin-off project from NCCS task 9. To achieve this aim, we will utilise a well-exposed faulted carbonate sequence from the Maltese Islands and link any fault controls with documented aquifers and any difference in hydraulic heads (Barbagli, 2021). To analyse the faults previously studied. we will create a realistic geological framework model of the islands in T7 based on mapped structure and stratigraphy. This model will be used as the framework to a geocellular model where the modelled formations are given physical properties. Afterward an algorithm will be run and give the modelled faults different properties. Next, attributes of faults that are known to be bounding different aquifers on the islands will be compared and contrasted with faults that are not. The values predicted by the algorithm will be used in a hydrogeological model. Here, observed water head will be compared to computed water heads when predicted values are applied.

1.3 Theory and previous studies

1.3.1 Previous studies

Compared to studies done on fault in clastic reservoirs, there has been little conducted on carbonate fault zones (Agosta et al., 2007; Billi et al., 2003; Cooke et al., 2019; Solum & Huisman, 2017) and even fewer have established an algorithm predicting transmissibility/permeability for carbonate fault zones. The ones that are developed are generally only applicable to the locality they are developed (Michie et al., 2018) Previous studies have confirmed that carbonate fault rocks can have sealing properties, conduit properties, or a combination of both relying on different factors such as displacement, host-rock properties and subsequent fracturing in the fault damage zone and fault core (Agosta et al., 2007; Billi et al., 2003; Celico et al., 2006; Michie et al., 2018, 2020). Through these studies, some relationships have been discovered. For example, it has been documented that carbonate rocks with low initial porosity tend to fracture and increase permeability (Billi et al., 2007). While carbonates with high initial porosity tend to have pore collapse and cataclasis, and an overall decrease in permeability (Tondi, 2007). This is similar to what expected from porous siliciclastic rocks.

1.3.2 Fault zone architecture

Previously established classifications of fault zones were developed by the investigation of siliciclastic and basement rocks. A fault zone architecture has been classified as a deformed fault core surrounded by a damage zone, with reduced deformation intensity in damage when moving away from the fault core and in to a little to no deformed host rock (Caine et al., 1996; Chester & Logan, 1986; Hausegger et al., 2010). However, a fault zone often shows complexity when observed in the field, with significant variability in the architecture and geometry.

Fault core is a complex structure and the area of a fault with the highest accumulated displacement (Caine et al., 1996). How the fault core is deformed depend on multiple factors. Studies suggest host rock, fault displacement, mechanical layering, and depth of deformation to be some of the factors impacting the deformation style of the fault core (Bastesen & Braathen, 2010). A fault core typically consists of one or multiple slip surfaces and lenses of fault rock. Depending on the percentage of fragments or matrix in the fault rock, the fault core can be classified as breccia, fault gouge or cataclasis (Sibson, 1977). It has been observed that for a fault core in carbonates to form the fault must at least accommodate a displacement of >1 m and for the fault core to be continuous it must be displaced > 5 m (Micarelli et al.,

2006). However, due to the different mechanical properties in some carbonate rocks, displacement is accumulated by several smaller slip surfaces, called a Fracture Splay Zone (Michie et al., 2014). This creates several smaller and independent fault cores and hence a greater throw is required to form a continuous fault core.

A damage zone is typically located on both sides of the fault and is categorized as secondary faults with little to no displacement, creating a network of fractures generally related to fault growth (Hausegger et al., 2010; Kim et al., 2004). Complications to this generalised fault zone architecture are observed. One key influence on altering the fault zone architecture is mechanical stratigraphy (Ferrill et al., 2017; Ferrill & Morris, 2008). Mechanical differences have been found to strongly affect factors such as faut core and damage zone width, propagation rate, failure mode, and nucleation points (Ferrill et al., 2017), which all influences the fault zone architecture. Mechanical differences are also important in carbonates. Observations show that for faults in massive limestone with low clay content tend to develop steeper dipping faults (>70˚) and in weaker limestones with higher clay content tend to develop shallower dipping faults (< 60˚) (Ferrill & Morris, 2008). Other observations made is development of a fracture splay zone (FSZ) due to mechanical differences between the stronger grain-dominated carbonates, and the weaker micrite-dominated carbonates (Michie et al., 2014).

1.3.3 Fault seal mechanisms

In order to predict the sealing potential of a fault it is fundamental to understand the processes that may create a permeability barrier (Knipe et al., 1997). Five groups of different processes have been identified to create sealing properties in faults. These groups can both create a seal on their own or in combination with the other groups.

The first process is porosity collapse caused by deformation related processes such as disaggregation, mixing and small-scale grain boundary sliding, which is typical for deformation at shallow depth of burial (Knipe et al., 1997). The next process is called diffusive mass transport. This is what happens when areas of high stress causes material to redistribute by dissolution, transport and precipitation (Mullis, 1993). The third process that can cause a low permeability is cataclasis. This happens when grains reduced and crushed by fracturing are grouped together (Sibson, 1977). Cementation is another way to lower the

permeability. This happens when faults act as conduits during faulting and allows fluids to migrate along the fault zone. The fluid increases the chance of mineralization, which will reduce pore space in the rock. Lastly it is smearing of clay, phyllosilicates or marls that creates a low permeable membrane along the fault plane (Lindsay et al., 1993).

Based on these processes fault seals can be divided in two broad categories: juxtaposition seals or fault rock seals (Knipe et al., 1997).

Juxtaposition sealing is a fairly simple concept relying on the lithology to create a seal. This happens when a unit of high permeability has been displaced by faulting by a unit of low permeability causing a barrier for fluid migration (Knipe et al., 1997; Yielding et al., 2010).

Fault rock sealing is associated with more complex processes primarily dependent on the host rock, deformation process, and condition experienced during deformation, such as temperature and stress (Yielding et al., 2010). Seals created by fault rocks can further be placed in smaller sub-divisions such as: cementation, dissolution, cataclasis, and smearing.

1.3.4 Permeability, Porosity, and transmissibility multipliers

The controlling factor whether a fault will act as a barrier, conduit or a combination of conduit and barrier depends on the relative contribution of fault core and damage zone to fluid mobility and is important when considering fluid flow in the subsurface (Caine et al., 1996; Michie et al., 2014). Fault permeability is a measurement of the ability of a fluid to flow through a rock, while transmissibility multipliers are used in numerical simulations instead of permeability (Manzocchi et al., 1999). As mentioned above, there are several different algorithms predicting permeability in siliciclastic fault zones, such as the shale smear factor (Lindsay et al., 1993), clay smear potential (Lehner & Pilaar, 1997) and the shale gouge ratio (Yielding et al., 1997). Since the algorithms is clay related, they do not take the chemical reactivation and differing deformation style of carbonates into account, and hence the aforementioned algorithms genetally cannot be used to predict fault seal in carbonate lithofacies.

Permeability

Fluid flow in the subsurface is controlled by multiple controlling factors and one of the most important is the rocks ability to let fluids flow through it. This can be expressed as the

observable measurement called permeability (Bense et al., 2013). The permeability of a fault zone can be influenced by several factors such as host rock properties, faulting, deformation, and fracturing. The understanding of how faults impact the fluid flow in the subsurface has gained much attention the last few decades (Faulkner et al., 2010). The classical model of a fault zone with a fault core and a surrounding damage zone is used to show how a fault ideally acts as both a conduit and a barrier for fluid flow. Here the fractured nature of the damage zone increases the permeability as it creates more pathways for the fluid to flow along strike. The fault core on the other hand often acts as a barrier. This is because the core consists of an impermeable fine and crushed grains in the fault gauge as well as clay smearing along the fault plane (Bense et al., 2013).

Transmissibility and transmissibility multipliers

Properties such as fault permeability is a physical property that easily can be observed and measured in faults at surface level. In the subsurface this is not as simple; therefore, transmissibility and transmissibility multiplier has been developed (Manzocchi et al., 1999).

The transmissibility uses the permeability of two juxtaposed cells. The equation is given as:

$$Transmissibility = Ak/L$$

Where: A cross-sectional area of the juxtaposed cells, k is the permeability, and L is the length between the two cell centres.

The permeability k is often given as a representative permeability between the footwall- and hanging wall cell. When it is no fault zone this is given as:

$$\frac{1}{\bar{k}} = \frac{1}{2k_{fw}} + \frac{1}{2k_{hw}}$$

Where: $\bar{k}$ is the mean permeability, and k_{fw} and k_{hw} is the permeability of the footwall and hanging wall

A similar equation is used to estimate the mean permeability of a fault zone. This is given as:

$$\frac{1}{\overline{k_f}} = \frac{1 - ({}^{t}/_{L})}{2k_{fw}} + \frac{1 - ({}^{t}/_{L})}{2k_{hw}} + \frac{t}{Lk_{fz}}$$

Where: t is the thickness of the fault zone and k_{fz} is the permeability of the fault zone. The equation for the transmissibility multiplier, established by Manzocchi *et al.* (1999), is given by combining the mean permeability of the footwall and hanging wall with the mean permeability of the fault zone. This gives the equation:

$$\frac{\overline{k_f}}{\bar{k}} = \left(\frac{1}{2k_{fw}} + \frac{1}{2k_{hw}}\right) \Bigg/ \left(\frac{1-(t/L)}{2k_{fw}} + \frac{1-(t/L)}{2k_{hw}} + \frac{t}{Lk_{fz}}\right)$$

Where: $\frac{\overline{k_f}}{\bar{k}}$ is the transmissibility multiplier.

The equation uses estimation of fault-rock thickness, fault-rock permeability, and surrounding cells permeability and size. However, similar to the other methods, this equation is limited to siliciclastic faults. This is because it uses an estimate for fault-rock thickness and permeability, and such method is yet to be developed for carbonates.

Shale smear factor

Shale smear along the fault surface decreases permeability across the fault, but for the shale smear to act as a barrier it is key that it is continuous throughout the entire fault plane. For the formation of shale smear it is crucial that the fault offset is developed across a mechanical weaker shale/clay layer (Færseth, 2006). One of the methods used is the shale smear factor, $SSF = \frac{T}{t}$ developed by Lindsay *et al.* (1993). This algorithm uses the ratio between fault throw (T) accommodated by normal faulting, and the thickness of the shale layer (t) to calculate a factor which indicates the probability of shale smear occurrence and continuous. Typical values which predict a continuous smear depends on the scale of the fault. For large scale faults visible on a seismic scale, a SSF value ≤ 4 indicates good probabilities continuous smearing. SSF values in the range 4-6 has a decreased probability of continuous smearing, and SSF values > 6 is interpreted as unlikely to have continuous smearing. In smaller faults (sub-seismic scale), the SSF values for continuous smearing can be much higher (Færseth, 2006).

Clay smear potential

Clay smear is low-permeable which forms as continuous bands in major fault zones. The smear is thinning away from the source bed and consists of mostly pure clay material (Lehner

& Pilaar, 1997). The second algorithm commonly used to find out if a fault is sealing or not is the clay smear potential (CSP). The definition of CSP is $\sum \frac{Thickness^2}{Distance}$, where the thickness is of a shale/clay bed and the distance is the throw accommodated by normal fault for that specific bed (Vrolijk et al., 2016). CSP values only gives indications of continuous clay smear. In a quantitative study Fulljames *et al.* (1997) gathered data from 91 reservoir along 10 faults in three different fields. In this study they found an increasing CSP values has an increasing probability of continuous clay smear up to a certain value where the CSP becomes independent of CSP (Fulljames et al., 1997).

Shale Gouge Ratio (SGR)

Unlike the two algorithms above the shale gouge ratio does not only consider thickness and throw distance of individual beds, but rather a sequence of beds in a given area of the fault (Yielding et al., 1997). The SGR can be given by two different equations. The first equation is a simplified equation with the assumption that the shale/clay bedding contains 100% shale or clay, and the other beds contain 0% shale or clay. This equation is given as $SGR = \frac{\sum Thickness}{Throw} \times 100\%$, where the thickness is the thickness of all the shale beds summed together divided by the throw accommodated by the fault. It is then multiplied by 100% to get the likelihood of shale gouge in percentage. The second equation is an extended version of the previous equation, where the possibility for shale/clay content in all beds are taken into the account. This equation is given as $SGR = \frac{\sum(V_{Shale} \times thicness)}{Throw} \times 100\%$. $\sum(V_{Shale} \times thicness)$is the content of shale/clay in each bed multiplied by its thickness. This is done for each of the beds in a sequence which is then divided by the throw of the fault and multiplied by 100%. A SGR above 20% is found to be the minimum value for a fault to be sealing (Yielding et al., 1997).

Permeability control in carbonates

A few studies in the recent years have been conducted to increase knowledge about controlling factors in carbonate fault rock permeability. These studies show the effect of deformation mechanisms, fault displacement, strain and juxtaposition permeability. There are three main classifications of the effect of faults on fluid flow in carbonates (Matonti et al., 2012).

Barrier/seal: with low permeability, high cementation and deformation, and low fracture frequency at metre scale. The existing fractures are not connected, hence it hampers the fluid flow the fluid flow. This creates a barrier which prevents across-fault fluid flow

Conduit/Drain: low to average cementation and deformation, high porosity, and fracture density. The fractures are connected in such a way that it enhances the fluid flow. This allows the fluid to flow easily across faults

Mixed: thick fault core with low permeability fault rock, high deformation, and cementation, creates an impermeable band which prevents fluids to flow across faults. High fracture density which is well connected on one side of the fault enhances fluid flow along strike of the fault.

Studying the undeformed host rock is important when exploring key parameters that may impact the sealing capacity of carbonate faults. Studies have been conducted (Cooke et al., 2019; Michie et al., 2020), focusing on how host rock porosity impact fault rock permeability. Samples of high porosity (>10%) and low porosity (<10%) host rocks were collected and compared to their deformed fault rock. Here, a trend was found that high porosity host rock tends to decrease in permeability and porosity as they are faulted, while low porosity host rock tends to experience a slight increase in permeability and porosity. One reason for that could be that high porosity host rocks have enough space that the pores within the rock can collapse, even under fairly low pressure and temperature. This, combined with cementation has the potential of decreasing the permeability of the fault rock with a magnitude order of eight (Cooke et al., 2019). This is not the case in low porosity host rocks. They need higher pressure for pores to collapse. Since compacted rock can withstand higher pressure, the rock tends to experience brittle failure, and fracture creation. This leads to an increase in permeability and porosity compared with the initial host rock. It is important to note that this porosity-permeability relation is relative to initial host rock porosity and permeability. Even though the high porosity host rock can show a decrease in permeability over several orders of magnitude, this may not mean that the absolute permeability is lower than the low porosity host rock, which increases in permeability (Michie et al., 2020).

1.4 Hydrogeology

An understanding of how faults in carbonate aquifers impact the fluid flow is an important factor to take into the account to best exploit the aquifers (Celico et al., 2006). In some cases, the fault core is known to cause an impermeable barrier to fluid flow, and the surrounding damage zone is documented to play an important role in fluid migration as it is often found to increase the fluid flow (Agosta et al., 2010). In addition to this carbonate rocks are prone to dissolution in water, leading fractures to expand and create karsts (Andre & Rajaram, 2005). Other structures that may cause horizontal flow anisotropy are anticlines, synclines and uplifted bedding where sub-vertical joints are dominant and juxtaposition against an impermeable formation (Billi, 2005).

2 Geological background

2.1 Study area

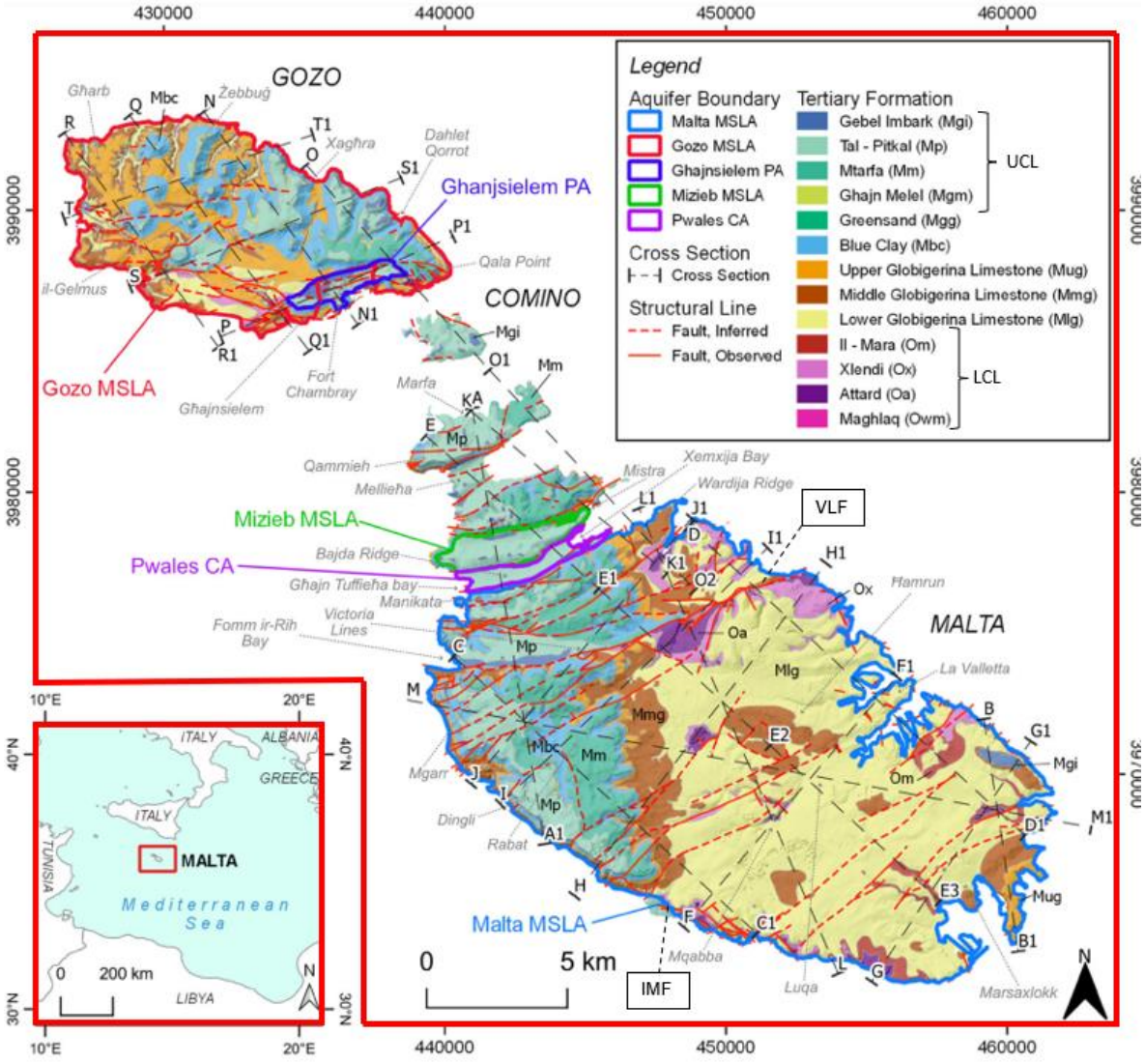

Fig. 1 Geological map of the Maltese Islands modified from Barbagli et al (2021)

The Maltese Islands are located in the Mediterranean Sea, 80 km south of Italy (fig.1). The area of interest is the Islands of Malta and Gozo because of excellent outcrop exposure allowing for previously documented detailed field mapping to be utilised for framework modelling. Further, Malta can be used as an analogue to the Smeaheia CO_2 storage site, associated with the marls within the sequence. The documented hydraulic heads of different aquifers across Malta and Gozo, can indicate which faults are sealing, and which are not.

Hence, utilising the known hydrogeology data with outcrops of the sealing or non-sealing faults can indicate the key controls on fault seal in a carbonate succession.

2.2 Geological background

2.2.1 Tectonic settings

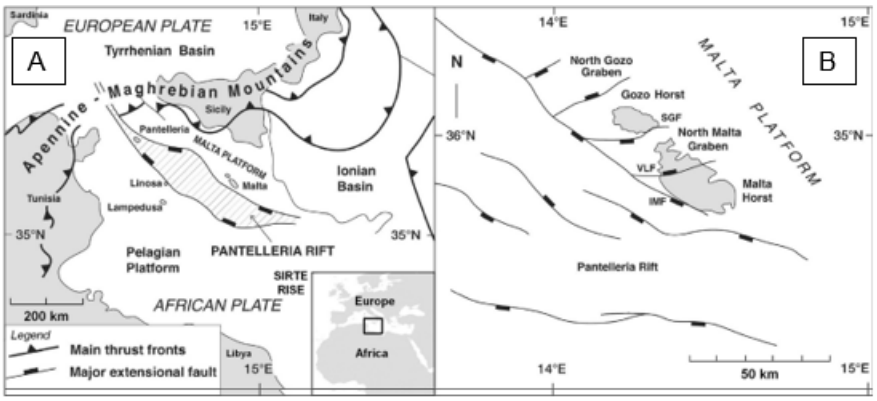

Fig. 2: A) shows the Apennine-Maghrebian fold- and thrust belt. B) zoomed inn on the Maltese Islands. Modified form Dart et al (1993)

The islands of Malta and Gozo are located in the Maltese graben system, a small part of the Pantelleria transform fault (fig.2A), also called the Strait of Sicily, caused by extension in the foreland of the Apennine-Maghrebian fold- and thrust belt (Argnani, 1990; Dart et al., 1993). They are dominated by extensional faults predominantly trending ENE-WSW. The islands are divided in to three distinct tectonic units (fig.2B), the Gozo Horst, the Malta Horst, and the North Malta Graben created by the South Gozo Fault (SGF) and the Victoria Lines Fault (VLF)(Dart et al., 1993).

In southern Malta there is an ESE-WNW trending fault called the Il Maghlaq Fault is observed in the southwestern edge of Malta. The overall structure of this fault is relatively simple as it is a relatively straight fault array with up to 2 km long fault segment. It has two principle slip surfaces with a fault core consisting of different types of fault rocks. Around the fault core there is a heavily deformed damage zone varying from 5 to 40 meters in width (Bonson et al., 2007). However, the fault also has areas of more complex structures located at branch-lines and where the traces of the fault bends. This fault is especially important as it is considered as one of the bounding faults of the Malta Mean Sea-Level Aquifer and will be one of the main faults I focus on within this study.

Although the faults systems are almost perpendicular to each other, analysis of sediment thickness related to fault displacement show that the faults have a relatively similar tectono-stratigraphic development, meaning they have been active at the same time (Dart et al., 1993). The stratigraphic history is described in four stages. The first stage, called the pre-rift phase or pre-rift strata, started in pre-Miocene and lasted to Triassic time. Formation deposited in this phase is defined by parallel bedding, which later has been tilted due to tectonic forces. In this stages Lower Coralline Limestone and the Lower Globigerina Limestone Formation were deposited. The next stage is the early syn-rift stage lasting from early-Miocene to Pliocene. Bedding is getting a slight variation in thickness, wedge shaped thickening toward south, related to fault displacement. During this stage members and formations such as the Middle Globigerina, Blue Clay Formation, Greensand, and lower parts of the Upper Coralline Formation was deposited. The third stage last throughout the Pliocene and is called the late Syn-rift. Here the majority of fault growth took place which can be recognized by localized areas basin depositions and non-depositional areas. Strata from this time period is absent on both Malta and Gozo due to a significant relief in the Pantelleria Rift and North Gozo Graben prior to reflooding. The remaining part of the Upper Coralline Limestone was deposited in this stage. The last stage in the stratigraphic history lasting from the end of the third stage and is still going today. Here the deposition is no longer offset by faults and is much smoother than the underlying structures (Dart et al., 1993)

The faults outcropping on the islands have an average dip between 64°- 73° (but has a broad range of values from 43°-90°) and a throw ranging from small centimetre-scale to large scale faults with a throw reaching hundreds of meters (Dart et al., 1993).

2.2.2 Stratigraphy

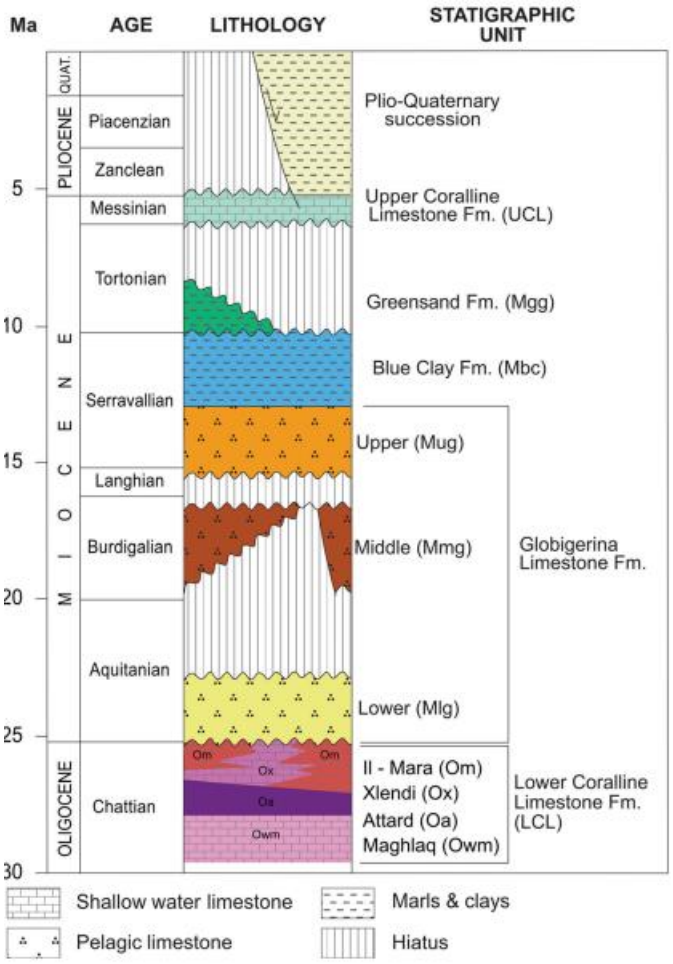

Fig. 3 Stratigraphic log of the Maltese Islands. From Dart et al (1993)

The islands are composed of five formations forming a relatively layer cake stratigraphy (fig.3). From oldest to newest the formations are the following: Lower Coralline Formation (LCL), Globigerina Limestone Formation (GL), Blue Clay Formation (BC), Greensand Formation (GS), and the Upper Coralline Formation (UCL). Four of the formations exists in large parts of both Malta and Gozo (LCL, GL, BC and UCL), while the fifth formation (GS) is mostly eroded and only appears in small areas, so it will not be takin into the account in the model.

Lower Coralline Limestone Formation:

Lower Coralline Limestone Formation is the oldest formation and hence occurs at the bottom of the stratigraphy on the islands. It is a pre-rift deposit, formed during the Oligocene and can be found throughout both Malta and Gozo (Dart et al., 1993; Pedley et al., 1976). The formation is divided into four members where the lower parts of the LCL characterized by a massive pale-yellowish bedding with biomicrites rich in benthonic foraminifera is the

Maghlaq mb. The second member of the formation is the Attard Mb. This can be recognized by it pale-grey coloured bedding with coralline algal limestone. Toward the top the Xlendi Mb. marks a change from the algal rich limestone to a coarse bioclastic limestone. To mark the top of the formation a fossil called *Scutella Subrotunda* is used, it is found in the tabular pale-cream to pale-grey beds of the Il-Mara Mb, which is only present locally in northern- and eastern Gozo, near the Qala Point. Through offshore studies the formation is recorded to be up to 1000 m thick, but the thickest observed thickness of the outcropping LCL is along the cliffs of the south-western coast of Malta and near Xlendi on Gozo and is measured to be 140 m. The initial deposition environment is interpreted to be shallow gulf environment, but progressively changes upwards in the stratigraphy to be an open marine environment (Pedley et al., 1976).

Globigerina Limestone Formation:

The second formation is the Globigerina Limestone Formation, a wackestone deposited during Miocene time. This is the formation with the largest surface area on the islands and is usually pale yellow with sequences of pale grey. It is divided in to three members, Lower- (LGL), Middle- (MGL), and Upper Globigerina Limestone Formation (UGL), separated by two conglomerate marker beds. The LGL can be recognized by its pale-yellow coloured massive beds of globigerinid biomicrites, which is thinning towards north-western Malta. To cap the LGL is the first conglomerate layer. Sandwiched between the two conglomerate beddings is the MGL, which starts directly above the first conglomerate bed. The MGL is recognized as pale grey Globigerinid biomicrites. Due to erosion most of this member is absent in the central parts of Malta. The last member is UGL which starts above the second conglomerate layer. This can be recognized by a sequence of pale yellow Globigerinid biomicrites in top and bottom of the member, which is divided by a pale grey marly biomicrites. In total the formation measures a maximum thickness 207 m around Marsaxlokk in sothern Malta but can be as thin as 23 m near Fort Chambrey in sothern Gozo. The depositional environment is interpreted to be at relatively shallow depths of 40-150 m (Pedley et al., 1976).

Blue Clay Formation:

Above the Globigerina Limestone is the third formation in the visible stratigraphy of the islands, which is called the Blue Clay Formation. The start of this formation can be

recognized by a one-meter short transition zone where it changes from globigerinid biomicrites to globigerinid marls. It is alternating light to dark grey in colour. Another recognizable feature for the formation is that it has a relative low carbonate content and at no point a higher percentage of carbonate then 30%. It also has a relative high percentage of phyllosilicates with it being up to 75% (John et al., 2003) North-eastern Gozo and western Malta has the thickest measured areas of the formation of ca. 65 m, which is thinning towards the south. The thinnest measured thickness is less than 20 m, where it is not completely absent/eroded such as in the eastern and southern parts of Malta.

Greensand Formation

The Greensand Formation is composed of a poorly cemented bioclastic limestone. The formation is highly bioturbated and is interpreted to be deposited under shallow marine. It is rarely thicker than one meter throughout Malta and Gozo but is locally recorded to be as thick as 11 meters near Gelmus, Gozo (Pedley et al., 1976).

Upper Coraline Limestone Formation:

The last and youngest formation in the stratigraphy is the Upper Coralline Limestone Formation (UCL). The naming comes from its similarity to the LCL both in colour and content of coralline algal. The preserved thickness of the UCL is 160 m and the deposition happened both during early- and late syn-rift stages in the Miocene. This formation has a more complex deposition history, with broad variation both vertical and horizontal in the lithology. Three different depositional environment divides the formation in to three sequences showing an increase in turbulence toward the east. Coralline algal bioherm represent a calmer bottom environment, above is a coralline rich patch reef deposition and at the top slightly eastly dipping cross-bedded limestones indicates more of a tidal delta/platform deposition. The formation can be divided into four members. At the base of the UCL is the Ghajn Melel Member, this is a foraminferal packstone with massive dark to pale brown bedding. Next is the Mtarfa Member, which contains thick beds of both carbonate mudstones and wackestones. It is yellow in colour in the bottom parts and gradually turns white and chalky toward the upper part. The third member is the Tal-Pitkal Member. This is a coarse grained wackestone and packstone with a pale grey to brownish-grey colour. The last and uppermost member is the Gebel Imbark Member which only exist in small patches throughout the islands due to erosion. It is pale grey in colour and is composed of hard carbonates. It is

also found in an uncomforaty where it is deposited directly on top of the Globigerina Limestone (Pedley et al., 1976).

2.3 Hydrogeological settings

There are five aquifers on the islands (fig.1), divided into three groups based on where they are hosted (Barbagli et al., 2021; Lotti et al., 2021). The aquifers are hosted in the Lower- and Coralline Limestone, which are divided by the Blue Clay Foramtion and the Globigerina Formation. The primary permeability for the Upper Coralline Limestone and the Globigerina Formation is both quite high, being 41-45% for the Upper Coralline and 32-40% for the Globigerina. No data is available for the Blue Clay Formation, and lastly the permeability for the Lower Coralline Limestone is 7-20% (Barbagli et al., 2021; Stuart et al., 2010).

The first type of aquifers is the unconfined perched aquifer (PA). This is an aquifer hosted in the Upper Coralline Limestone and is floating on top of the impermeable Blue Clay formation. They are only present in Gozo and northern parts of Malta. In central and south-eastern parts of Malta, they are absent due to erosion of the Blue Clay.

Beneath the PA, divided by the Blue Clay, are the second type of aquifers. This is a freshwater body floating on top of denser sea water hosted in the Lower Coralline Limestone. These aquifers are locally called Mean Sea-Level Aquifer (MSLA). The main aquifers of this type are the Malta MSLA, the Mizieb MSLA, and the Gozo MSLA. These aquifers are considered as unconfined aquifers since they are predominantly hosted in the Lower Coralline Limestone and is mostly unaffected by the low permeable Globigerina Limestone (Lotti et al., 2021).

The third type of aquifers is hosted in the Upper Coralline Limestone faulted down to sea-level with Blue Clay underneath sea-level. This is the Costal Aquifers (CA). An example of this type of aquifer is the Pwales CA located between the Malta- and Mizieb MSLA (Lotti et al., 2021).

The main source of recharge for all the aquifers is precipitation, in addition there is some recharge from infiltration from dams and leakage from the water network. For the MSLA-aquifers recharge happens through water infiltration through fractures, faults and sinkholes. It

is also possible that there is some recharge from leakage from the perched aquifers (Lotti et al., 2021).

3 Method

3.1 T7

3.1.1 Faults of interest

Not all faults on the two islands are used in this study because the offset of the Blue Clay is not large enough to impact the aquifer. Hence, assessment must be done of all the faults to identify key faults for analysis. This is done by reviewing literature and geological maps of from the area to find faults of interest. The key faults were picked because of they are known aquifer bounding faults. Other similar, but not bounding, faults were picked to be as a comparison to the bounding faults. The two main faults used is the ENE-WNW striking Il-Maghlaq Fault located in the south-east and the E-W striking Victoria Line Fault crosscutting central Malta. These two faults are of similar throw with the largest segment having a throw >200 m. Three other faults were picked. The first on is a fault on Gozo, from now on and out called the Gozo Fault. This fault is picked as it is located at the northern boundary of the Ghanjsielem aquifer and may act as a barrier on this aquifer. The second fault used is a fault from the southern part of Malta. Here it is only the Globigerina Formation and the Lower Coralline Formation that is affected by the faulting as the above laying formations is eroded and is used to show how this impacts the fault. Last is the Pwales Fault, just north of the Victoria Line Fault. This is picked because it shows interesting results with regard to the shale smear.

3.1.2 Geological framework model

The framework model was created in the software T7. A geological map of Malta was downloaded from the Maltese government webpage, and a scanned geological map over Gozo was provided from the supervisor (Emma) along with a digital elevation model (DEM). The geological maps where draped and manually fitted to the DEM. This was done by matching easy recognizable features on both the map and the DEM. As shown in fig.22 in appendix A, the small half-islands and bays around the islands is visible in the DEM and possible to line up with the correct part of the map.

Next, the contact between formations on the geological map was used to trace out the top of each formation, effectively creating a top and base of each of the main formations: Lower Coralline Limestone, Globigerina, and Blue Clay. This gave the program enough data to be able to create a gridded surface of the formations. However, there are two exceptions. There is nothing that can be used to create a base for the Lower Coralline Limestone as it is not observed in outcrops. The second exception is the top of the Upper Coralline Limestone which also is not outcropping on the islands.

Next step is to trace out the previously identified faults. This is done in the same way as the formations, by using the geological map and trace out the faults of interest as segments. The fault surfaces are set to projected 1000 m up and down from the fault segment and have a dip of 67° which is the average dip value found in literature (Cooke et al., 2018; Michie et al., 2014). Next, these surfaces were assigned to the fault segments and dip direction was decided by using the symbol on the geological map. The interception between the horizon surface and the fault surface was then used to create polygonal lines for the foot- and hanging wall cutoffs, known as polygons. These polygons have been quality controlled my manually editing. This is done by correlating features on the geological map with existing cross-section created of the island.

The polygons used to create throw profiles along the length of the faults to aid with their quality control. Further quality control was done by using the throw distance plot of each fault. Here errors and irregularities according to fault theory is identified and fixed by tweaking the cutoff lines. In this way errors such as multiple throw centres are detected and improved, this is being described in more detail later.

Finally, the gridded horizons are converted to tri-mesh surfaces and fitted to the framework by extrapolating between the horizon interpretation and the polygon lines. Since no upper or lower limit of the geological section can be observed from the geological map, the horizon of the top Blue Clay is copied and pasted as top of Upper Corallin Limestone Fm and adjusted to an estimated high (assuming no change in thickness across the islands). The same is done for the base of the Lower Coralline Limestone, but this is pasted down to a lower boundary. A final boundary will be pasted an arbitrary 200 m above and below the final framework to ensure that the model juxtaposes sufficient layers.

3.1.3 Quality check

Each fault was inspected manually to see if the polygons correlate with fault theory. This was done by visualizing the throw on each fault surface. Areas of large accumulations of throw is marked in red. This should according to fault theory be toward the centre of the fault with progressively less and less throw accumulated toward the fault tips, creating a bulls-eye-pattern. Here the blue colour indicated low throw, green is intermediate, and red is maximum throw (colours are relative to minimum- and maximum throw of each individual fault). Some faults show multiple large throw accumulating centres (fig.4A), often indicating wrong interpretation. Faults where this were detected the polygons had to be tweaked till only there were only one centre (fig.4B). Further, when the geocellular model was created it was inspected for irregularities which could not have a geological explanation. This could be unnatural spikes in the cellular or unrealistic looking faults. When none of this was detected, the cellular model was ready for parameter population.

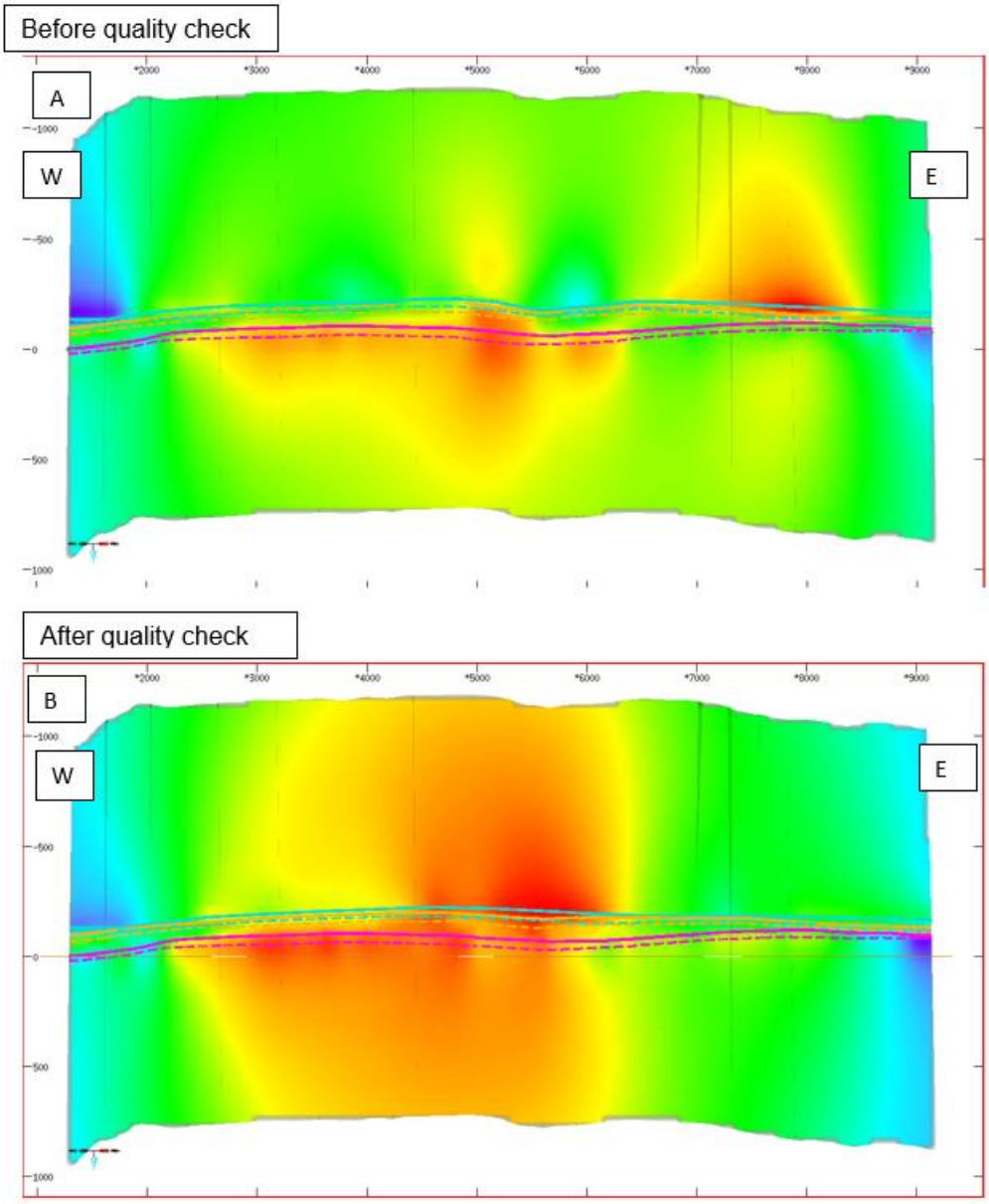

Fig. 4 A) Shows throw of fault with multiple throw centres before quality check. B) Shows the result after quality check

3.1.4 Geocellular model

After creation of a framework model, the next step was to create a geocellular model using the framework model. First, a grid with a cell size of 40x40 meters was stretched over the survey area. Next horizon trimesh, and pillar faults were added to create the volume of the geocellular model. The grid cell was set to 50% honour the faults (fig.5), this gives the cells the ability to change form and size to better honour the fault geometry making them more realistic instead of stair stepping. This can be seen in fig.5 where the cells surrounding the faulted area is distorted compared with the cells further away from the fault which is

completely squared. The island of Gozo is populated with three wells which gives the model properties. This includes V-shale ratio, porosity, net-to-gross, and permeability in x-, y-, and z-direction. The V-shale ratio, porosity and net-to-gross were all populated in the model as arithmetic mean. The permeability was supposed to be populated using geometric mean, but due to a bug in the software this resulted in negative values. Thus, harmonic mean was used instead. From the imported data the program could use built in algorithms calculate SSF, transmissibility multipliers, and permeability for the fault zone.

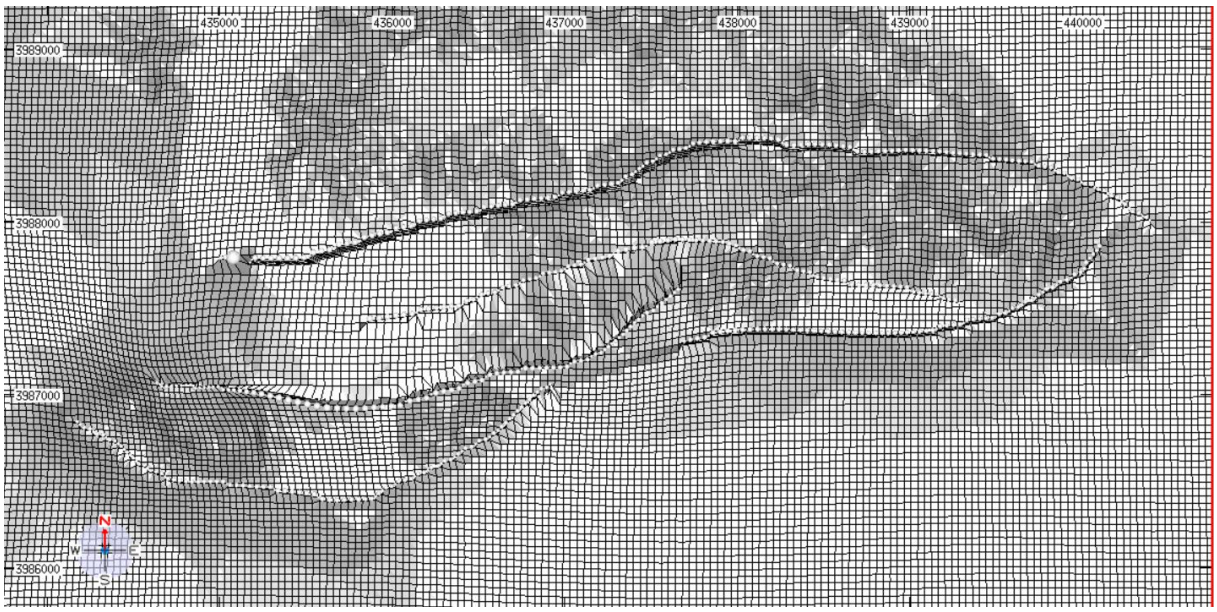

Fig. 5 example of how the grid cells is distorted around faults, from the Island of Gozo.

3.2 Hydrogeology

3.2.1 Well assessment

The well data provided by the Maltese Energy and Water Agency consisted of 17 excel-files. The was 16 wells included within the Malta MSLA and one well on Gozo. The excel-files contained water table data measured for 365 days along with the coordinates for the given well. No data north of the Victoria Line Fault was provided for Malta MSLA. The wells were plotted on a geological map (fig.6) using the coordinates provided. Wells which were located on each side of a fault was identified, and the water table for each well was checked against each other. In this way it was possible to identify weather a fault had an impact on the groundwater or not.

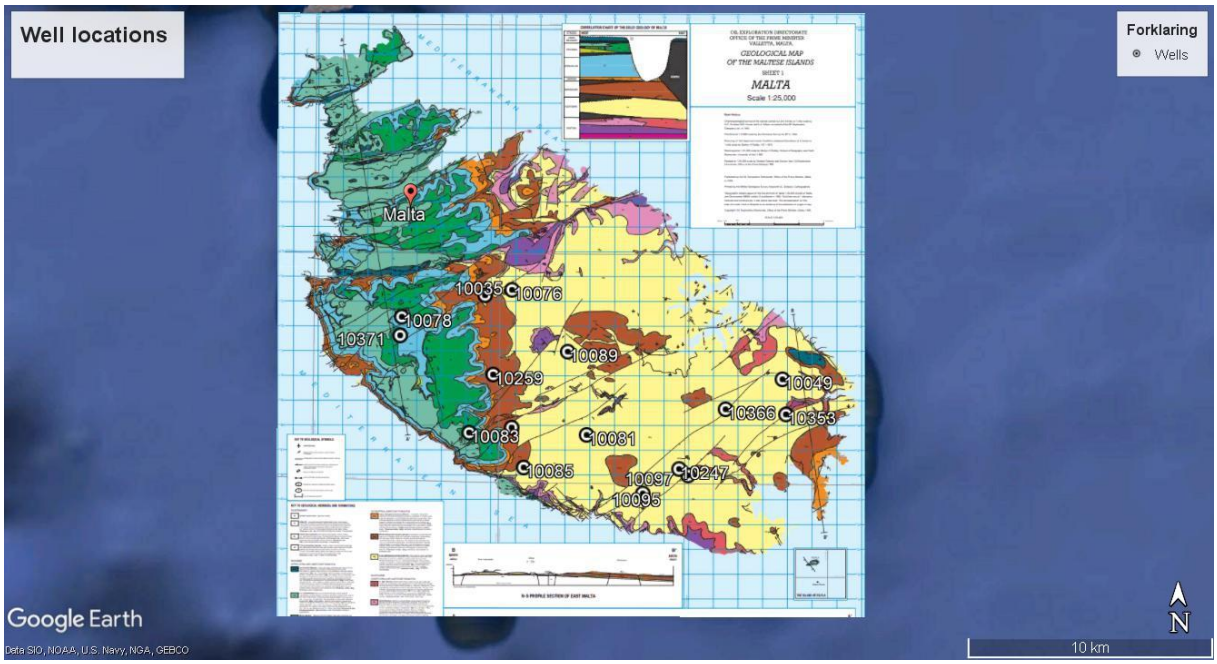

Fig. 6 Well locations plotted on geological map of Malta.

3.2.2 Theory of the numerical model

A simple one-layer numerical model was developed to simulate how the groundwater reacted when introduced to a fault. The data used for this model is gathered from literature studies, parameters from the fault modelling, and water table data provided by the Maltese Energy and Water Agency. This makes it possible to define model boundary, hydraulic conductivity, area porosity, and recharge values for the aquifer.

Hydraulic conductivity (K):

This is the capacity of a rock to transmit a fluid. There are several factors which influences the hydraulic conductivity. This can be the shape of the grains and heterogeneities in the rock or the nature of the fluid. Permeability (k) can be linked to the hydraulic conductivity through the equation:

$$K = \frac{k\rho_f g}{\mu}$$

Where:

k is the permeability

μ is the dynamic viscosity of the fluid

ρ_f is the density of the fluid

g is the gravity constant

Porosity:

Porosity is the volume within the rock which is "empty space" and not filled with any minerals or cement.

Recharge

This is the amount of water that manages to infiltrate through the unsaturated zone reaching and adding to the groundwater table. For the islands of Malta and Gozo the main source of recharge comes from precipitation and can be expressed by the equation:

Recharge = Precipitation - Surface Runoff - Evapotranspiration

Software

The program used for the modelling of groundwater flow is the Groundwater Modelling System (GMS) developed by Aquaveo, LLC. This program run input-data through common numerical groundwater models and creates a graphical visualization of the output-data. For this thesis the numerical model MODFLOW is used. This uses equations derived from Darcy's Law, which describes the rate of water flow through a porous earth material as:

$$Q = -KA\frac{\partial h}{\partial l}$$

Where:

Q is the water flow (m^3/day)

K is the hydraulic conductivity (m/day)

A is the surface area through which the water moves (m^2)

$\frac{\partial h}{\partial l}$ is the hydraulic gradient (dimensionless)

Since this is looked at as a steady state system all variables are constant except for the hydraulic conductivity making it the controlling factor for the water table in the model.

The modelling was approached by using a conceptual model. This is more convenient as all the data used is stored in coverages such as polygons, arcs, and nodes. By using this the data

automatically assigned the values to the grid of the model, instead of doing this cell by cell (Zhou & Li, 2011).

3.2.3 Model setup

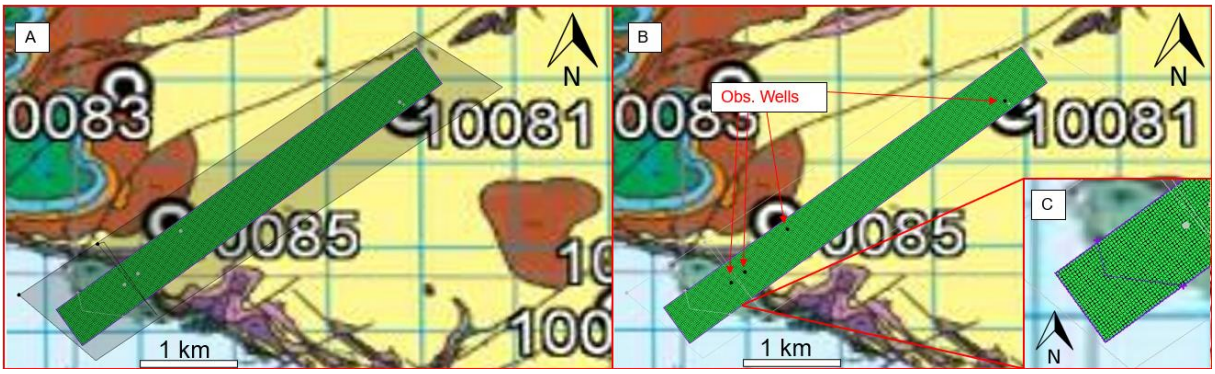

Fig. 7: shows boundaries of the modelled area. A) Green gridded area is the modelled area with the boundary of the grid frame around. The shaded grey area is the recharge and hydraulic conductivity polygon. B) Black dots are the locations of the observation wells. C) purple line is the specific head representing the sea.

The model was created by snipping a part of the geological map showing the Il-Maghlaq Fault with plot of the known wells. Afterward a conceptual model was created, and multiple coverages was added as boundary conditions to the model. The first coverage created was for the boundaries for the model, which also includes the hydraulic condition (fig 7A). A copy of this coverage was used for the recharge (fig.7A). Both these coverages are represented with a polygon created around the area of interest. The hydraulic conductivity coverage was divided into three zones representing the footwall, fault zone and the hanging wall. A coverage with specific head was created to simulate the sea, this is represented as an arc following the coastline on the base map (fig.7C). The known water heads from wells are set as observation wells to see how the simulated model fit with reality (fig.7B). This was then mapped to a 3d-grid which is 500 m wide, 5000 m long and 180 meter thick. The bottom of the grid is set to -150 m, meaning the top is at 30 m above sea level. The grid was then rotated 36 degrees to be perpendicular to the fault. This results in one-layer model divided in 25 x 250 cells. A new mudflow for the grid was created, checked for errors, and runed.

At the depth of the aquifer the two high hydraulic conductivity formations of the Lower- and Upper Coralline Limestone is juxtaposed against each other, giving the only making the fault the only source of fluid flow barrier. Multiple values in the range from 10-35 m/day was tried for the conductivity of the foot- and hanging wall. The fault is given by a 15 m thick zone where the hydraulic conductivity is lowered significantly. Here values in the range of 0.0001

– 1 m/day, arrived from T7, was tested. A variation of fault zone thicknesses was also tried to see how it impacted the model.

The recharge is assumed to cover the entire modelled area. The average yearly precipitation for Malta is 554,6 mm/year, and an average evapotranspiration is calculated to be 346,9 mm/year. Runoff for the island is not given so the available average of water for infiltration + runoff is 207,7 mm/year (Lotti et al., 2021). This is used as the input in the model but is probably lower in reality.

4 Results

4.1 T7

4.1.1 Geocellular model

The model predicts parameter for each of the cells in the geocellular grid. This includes each of the four formations stretching across the islands, and all of the 23 faults included in the framework model (fig.8). The parameters used for the entire cellular grid are permeability and v-shale values. For the faults there are six different parameters: shale smear factor, fault zone permeability, transmissibility multiplier, footwall-, and hanging wall permeability, and lastly fault rock thickness. The two main faults of interest are the Il-Maghlaq Fault and the Victoria Line Fault. Attributes from both of these two faults creates a possible explanation to why one of them is known to be an aquifer bounding fault, while the other is not. These two faults will also be compared to other aquifer bounding faults, and faults without impact on aquifers. The locations for the faults used in this analysis is shown in fig.8. Here we see that the Il-Maghlaq Fault is located at the south-eastern side of Malta. The Victoria Line Fault is located in central part of Malta with the Pwales Fault just north of it. The Gozo Fault is the northernmost fault used and lastly it is the fault I called the Southern Fault, located in the south of Malta.

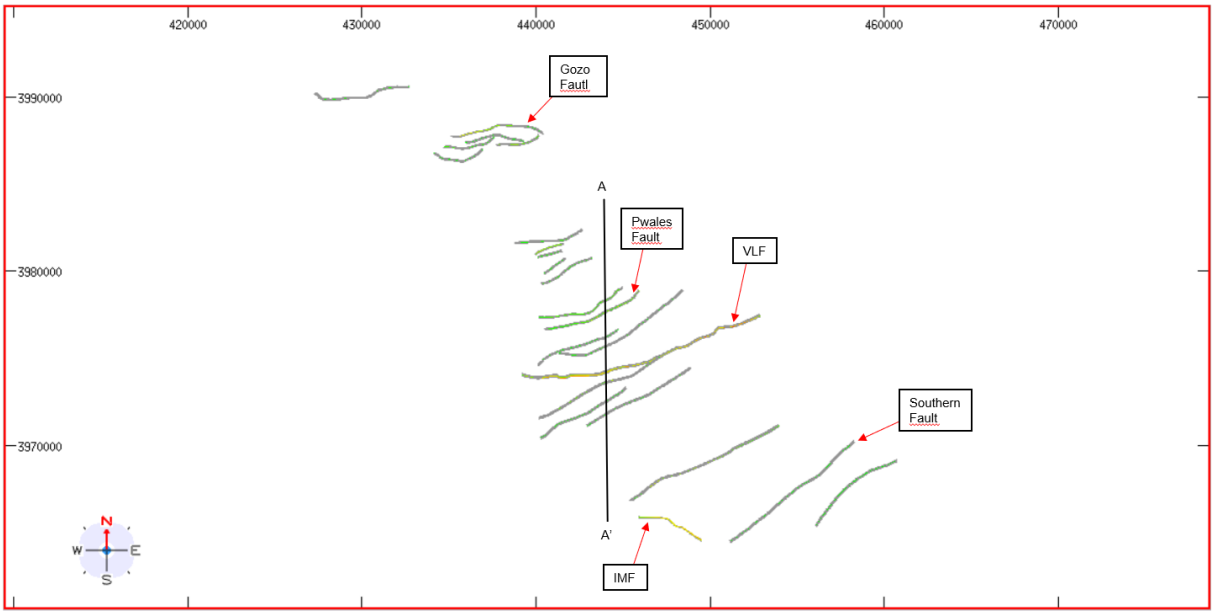

Fig. 8 overview of the faults analysed in this thesis. Black line is the cross-section in fig.9

Fig.9 shows a ~N-S trending cross-section of the geocellular model, and where faults displace different formations. It also shows how the thickness variation occurs throughout the model. Fig.9 shows the v-shale distribution through the model. Here we see where the Blue Clay is located in the model. Note the Blue Clay is thinning towards the south. In fig 9 we see the permeability distribution of each of the four formations. The uppermost blue to purple colour is the highly permeable Upper Coralline Formation. Underneath is the impermeable formation of the Blue Clay represented in orange. Next, is the Globigerina Formation which is the lighter blue colour and at last is the Lower Coralline Formation in dark blue and green, representing moderate and high permeability, respectively.

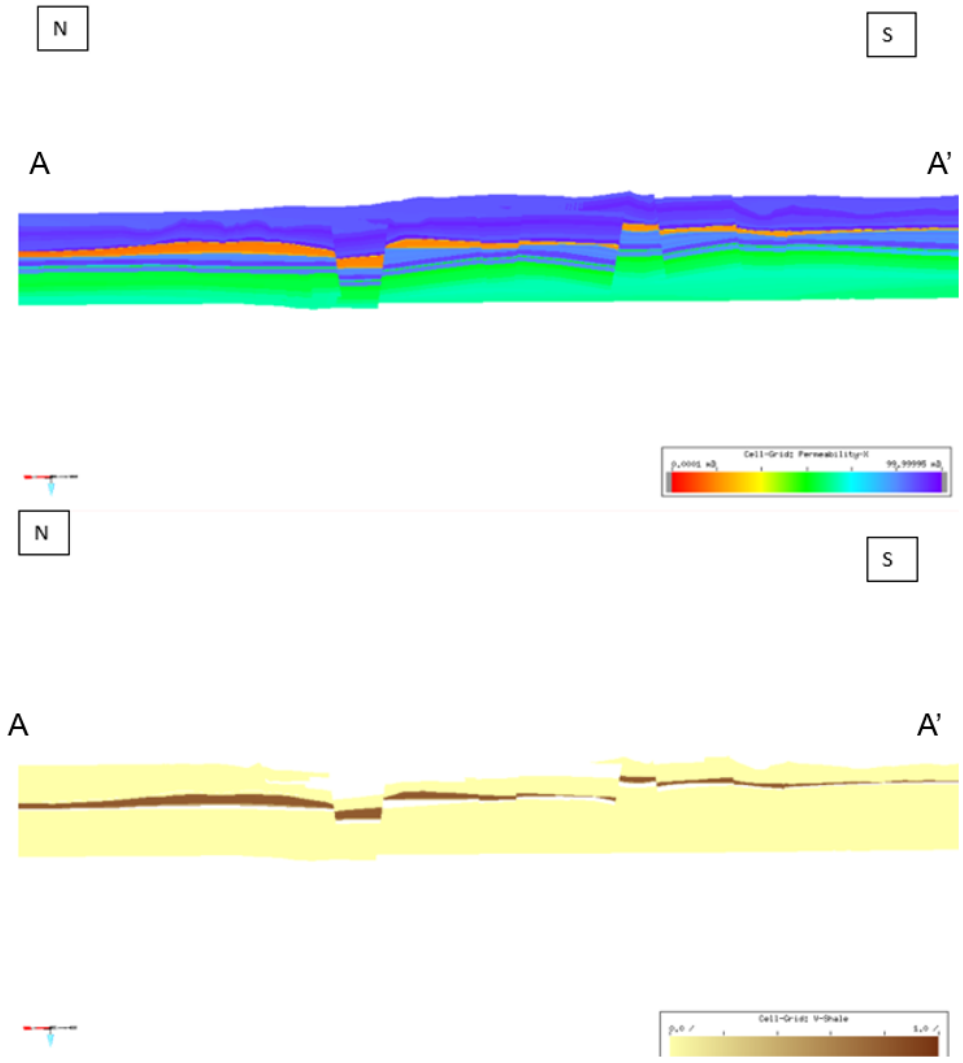

Fig. 9: N-S cross-section of Malta (fig.8) show the permeability of the layers. Dark blue is the UCL, orange is BC, blue is the GL, and green is LCL. Picture below shows same cross-section displayed with v-shale. Brown is the BC. UCL, GL, and LCL are displayed in yellow

4.1.2 Geocellular faults

SSF

The colour bar for the shale smear factors ranges from 0-10, where the colour transfer from green in areas of lower values, through yellow at intermediate values and ends up as red in areas of high values. The increments shown increases with a value of two for each step.

The Il-Maghlaq Fault shows a wide zone of shale smearing. Looking at the southern end of the fault, there is mostly an orange colour with a minor green at the bottom (fig.10A). The orange colour indicates a SSF of 5, and the green at the bottom is roughly 3. Moving toward the north, the overall colour is yellow to orange, indicating values between 4 to 5. At the very the north there is a sudden change in colour from yellow to green indicating a lowering of the value to around 2.

Where only the Lower Coralline Limestone is juxtaposed, we see that likelihood of shale smearing is predicted. The area with shale smear is observed to be fairly wide in the southern end, increasing toward the central part of the fault, but thinning significantly toward the north

The Victoria Line Fault shows a thickness change in the shale smear zone is from east to west; where the smear is thinner towards the east. Moving westward there is an increase in the width, before it thins out at the westernmost tip (fig.10B). There is an overall greenish colour indicating that there is in general low value on the shale smear factor. However, importantly, there are some areas and patches of a more yellow to orange colour, and even some smaller areas of red.

For the shale smear in areas of Lower Coralline Formation juxtaposed in the VLF we observe only a thin sliver at the top. Note, in the easternmost parts of the fault the shale smear is completely absent. The shear zone becomes thicker and roughly reaches depths of 0 meter above sea level (m.s.l.a) toward the west. From the central parts of the faults towards the western edge, the zone is thinning until almost completely absent.

The fault chosen from Gozo shows a shale smear zone which is thickest on the western side of the fault and is thinning toward east (fig.10C). It has a yellow to slightly orange colour in the thicker western area. It progressively transits into a green colour as the zone start thinning

Looking at the shale smear zone for the Pwales Fault there is a relatively thick zone of green colour (fig.10D), meaning a SSF between 0-2. In the eastern side there is a zone of higher values at the top of the SSF-zone. Form west to east we observe a thinning of the zone.

The southernmost fault has a wedgelike form, being thickest in the east and is thinning toward west (fig.10E). There is little to no variation of colour in the zone where shale smearing is possible. The overall colour is green indicating a high likelihood for shale smear.

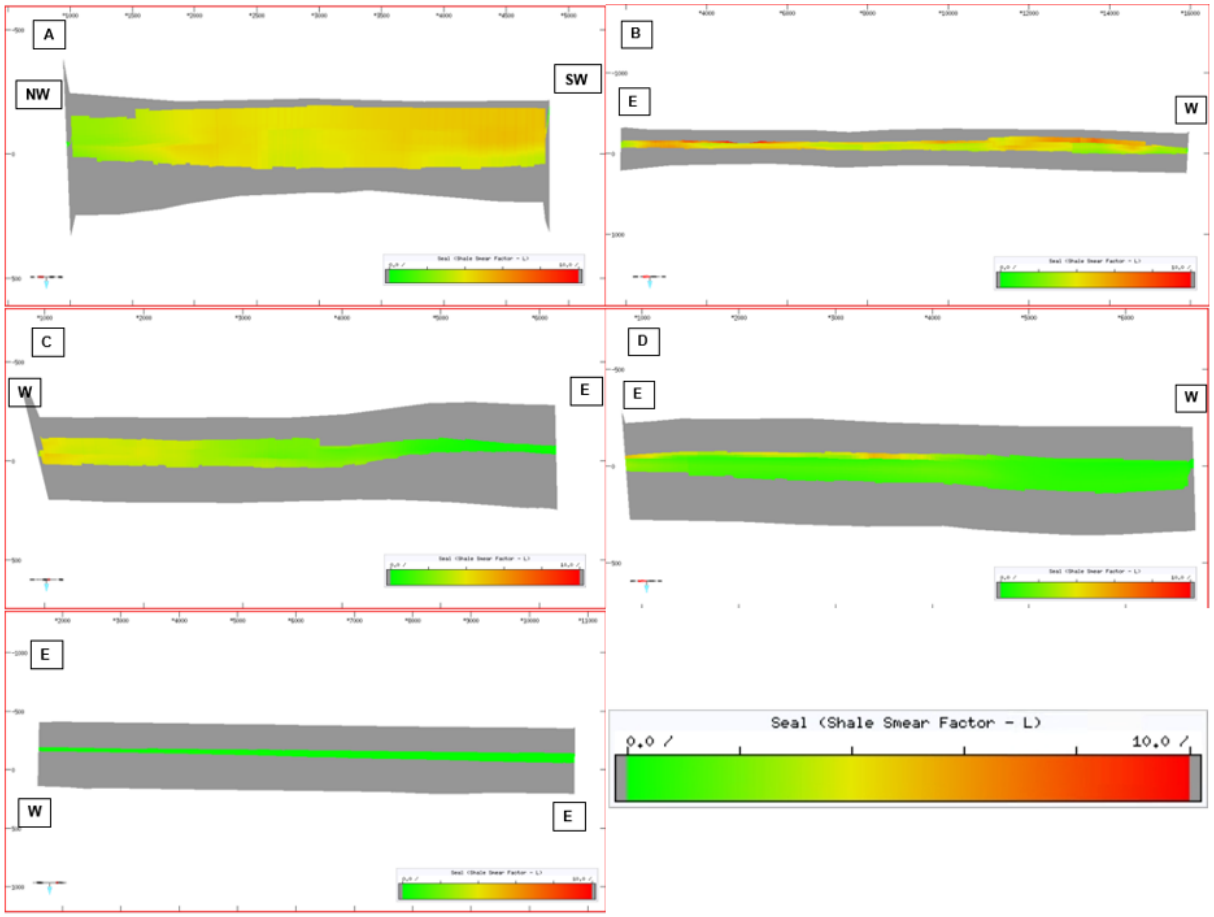

Fig. 10: shale smear factor displayed on the faults: A) IMF, B) VLF, C) Gozo Fault, D) Pwales Fault, and E) Southern Fault.

Frequency plots show the statical variation of the SSF for the three faults: Il-Maghlaq Fault, the Victoria Line Fault, and the Pwales Fautl (fig.11). Values for the SSF plotted are in the range between 0-15. Here we see that the values for the Victoria Line Fault have a wider range, calculated values are mostly in the range 2-6 but both lower and higher values are observed. For the Il-Maghlaq Fault almost all of the values calculated are ≥ 5. The Pawales Fault has most of its values under a factor of 2. However, some values are calculated as more, where most of them are ≥5, but a few are just above 5. Comparing the values to the SSF displayed on the faults we see that for the Il-Maghlaq Fault shows high values close to 5

scattered over most of the fault (Fig.10A), while for the Victoria Line Fault higher values is more concentrated to the top if the fault (Fig.10B). Here we also see values that far exceeds the cutoff value for shale smear. The Pwales Fault has mostly green values across the entire SSF, but a small area toward the top is calculated to have higher values (Fig.10D).

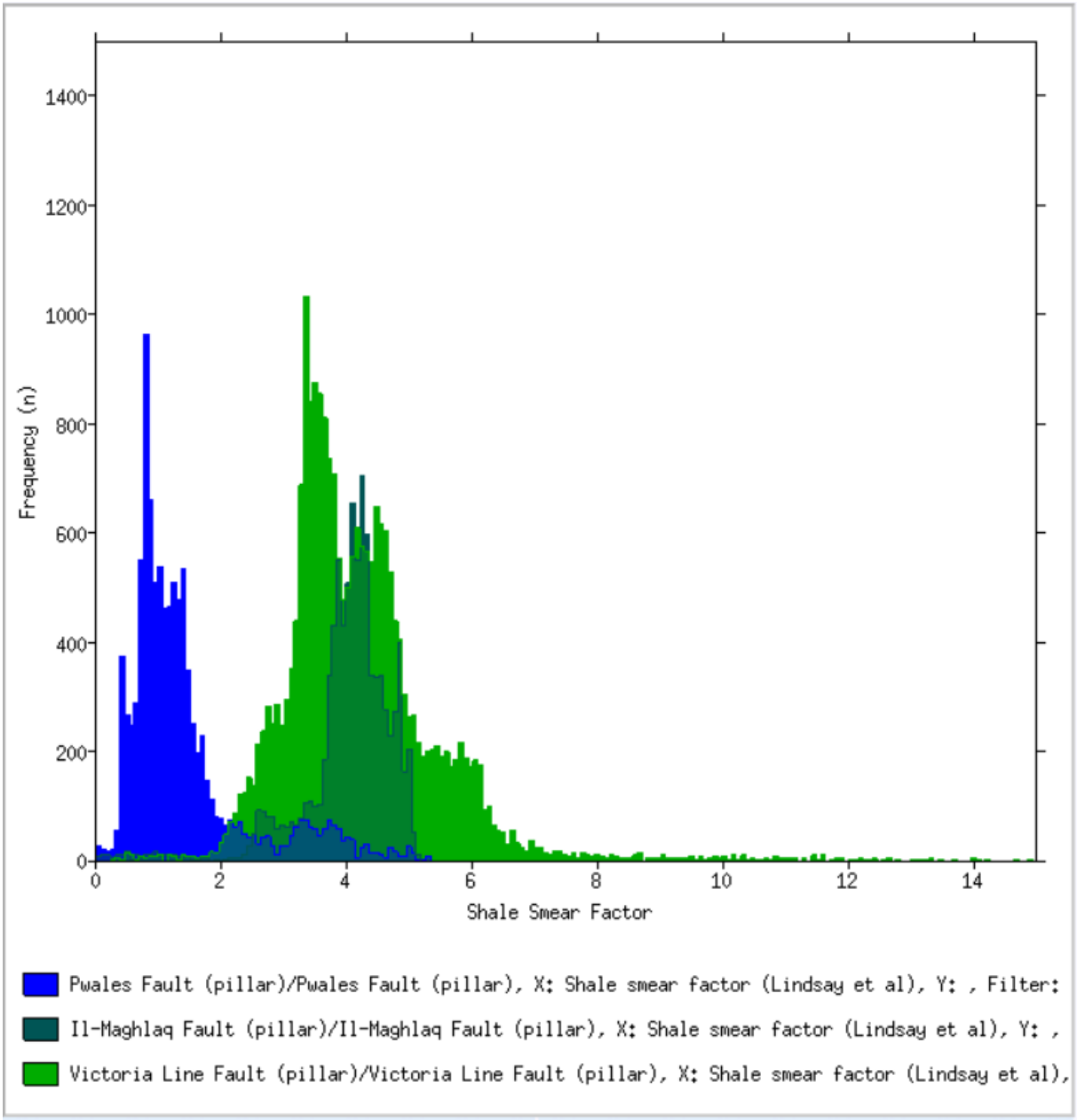

Fig. 11 Frequency plot of the three faults: IMF, VLF, and Pwales Fault

Permeability

The values for the fault zone permeability ranges from 0.0001 mD to 100 mD and is visualized with a rainbow plot where lowest values are red in colour and the highest values

are purple. The increments are logarithmic meaning each marker on in the colour bar has an increase of 10 times the last marker.

In the Il-Maghlaq Fault there is an overall decrease of fault zone permeability with depth. The colour transitions from light blue at the top and transfers in to yellow/green at the bottom of the fault. There are three distinct patches in the middle of the fault marked in red, indicating a very low value of permeability which is close to or at 0 mD (fig.12A).

Victoria Line Fault shows a similar pattern as the Il-Maghlaq Fault with a downward decreasing permeability in the fault zone. The colour goes from the same light blue to a yellow / green at the bottom. The model also shows a low permeability zone, observed as red patches (fig.12B).

Toward the top of the Gozo Fault, it is a light blue colour as in the aforementioned faults, with the same pattern of downward decreasing permeability. In the western side it looks to be an overall slightly greener colour, while at the eastern side has a slightly more yellowish colour. Most of the zone where the SSF was predicted has a red colour. A similar pattern as all the previous faults (fig.12C).

The Pwales Fault has similar pattern of light blue colour at the top, and green at the bottom. The red zone in the middle is thickest in the west and is thinning toward the eastern end (fig.12D).

The fault zone permeability of the southern fault shows the same downward decreasing permeability as the other faults. The colour has a laminating pattern switching between different colours. It starts off with light blue colour and transit gradually to green colour. Along the transition there is a laminating effect where thin zones of different colours are shown. It is not only transition from blue to green, but there is also the wedge-shaped form in the middle of the fault, which is completely red.

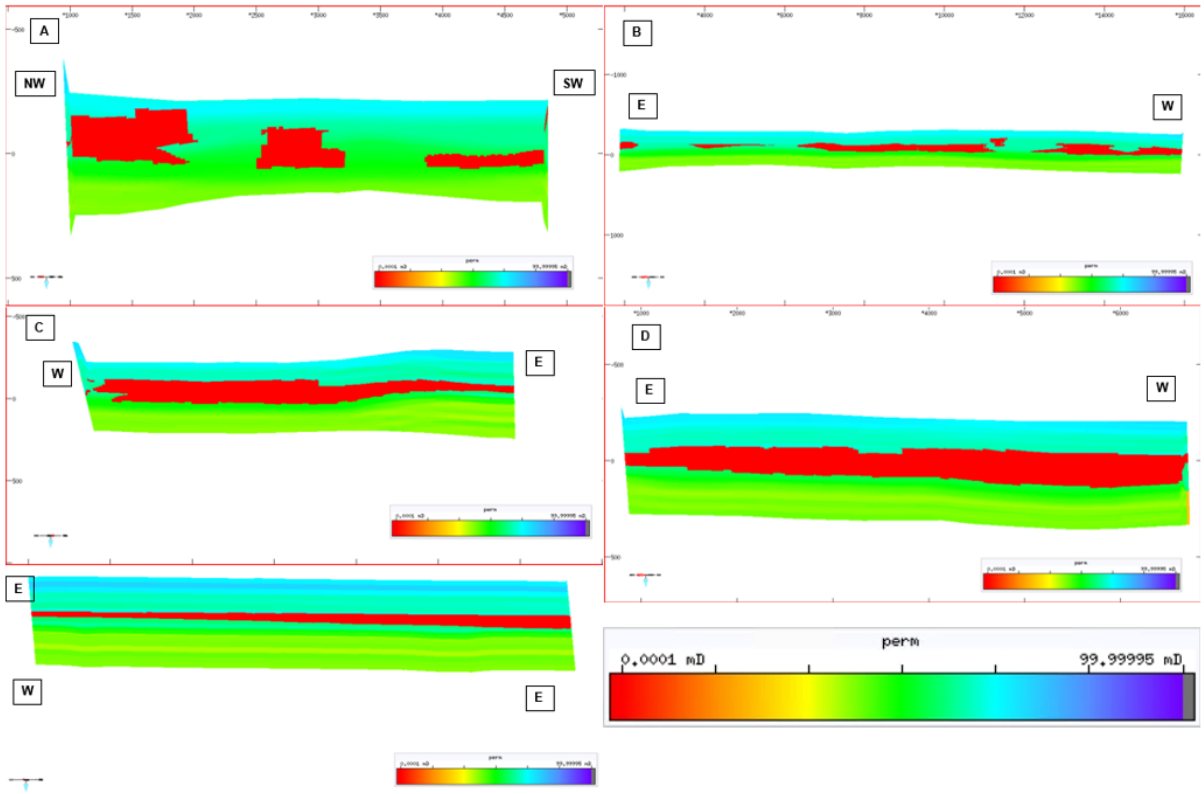

Fig. 12 permeability of the faults: A) IMF, B) VLF, C) Gozo Fault, D) Pwales Fault, and E) Southern Fault

Looking at the change in permeability for the fault plane in the footwall (fig.13) compared to the permeability in the hanging wall for the Il-Maghlaq Fault. In the footwall there is only a thin zone dark blue to purple colour indicating permeability close to 100 mD at the top which transfer over into a zone of lower permeability. This is observed by a change in colour to orange indicating a permeability of 0.001 mD. Underneath the low permeable zone there is a large increase again. Following the fault plane down dip the colour goes from blue to a darker blue indicating an increase in permeability. In the middle of the fault a sudden drop in permeability marked with a transition to a green colour, which correlates to a permeability of 0.1 mD, which stays the same all the way down to the bottom. In the hanging wall (fig.13) there is a much larger zone of high permeability at the top. The zone of low permeability is now in the lower half of the fault, still with the same orange colour. Underneath is the same increase which transition into the green values at the bottom.

The footwall side of the fault for the Victoria Line Fault has a high permeability in the uppermost part of the fault it has the same layer of low permeability as the Il-Maghlaq Fault (fig.13). This layer is in the middle of the upper half of the fault on the eastern side and is

propagating upward on the fault as we follow along the strike toward the western side before it dips down again at the absolute end. There is a thickness variation of the layer with it being thinner in the eastern side of the fault than on the western side. Underneath this layer there is a wedge-shaped area of blue colour with a permeability of around 10 mD. The same permeability is observed in a lens-shape on the western side. This is also observed between the two shapes, but it is much thinner. Next is a thin area of purple which quickly changes to green. In the hanging wall there is the same pattern with a high permeability zone above and below a layer of lower permeability. The high permeable layer above is thicker than in the footwall. The lower permeable layer is straighter in the hanging wall, but still shows a thickening from east to west.

The footwall and hanging wall of the southern fault looks almost identical. Both have a thick high permeable area on the top, with similar thickness. It is transferring into an area of dark blue. The colour is slightly brighter on the western side of the fault than on the eastern side. Next is the low permeable area. This has a wedge shape being thinnest in the eastern side of the fault and thicker toward the west. Underneath is again a high permeable area and the fast transition to the green (Appendix A).

Similar to all the other there is the same pattern with high – low – high permeability in the Gozo fault too. The interesting part here is the shape of the low permeability zone. In the Footwall it is fairly similar located on the fault in terms of depth. in the western part of the fault the thickness is relatively similar but moving eastward along strike there is a change. At approximately the centre of the fault the there is an increase of thickness in this zone, which thins and thickens again before it eventually thins toward the edge. Directly underneath the low permeable zone there is a zone of lighter blue colour. This has the opposite direction of thickening with it being thicker in the western side and thinning eastward. In the hanging wall the low permeable zone is much lower in the western side or the fault. Moving along strike to the eastern side there is a slight increase in the thickness close to the centre. East of this point there is a kink upward in the low permeable zone moving it closer to the area it is on the footwall side (Appendix A).

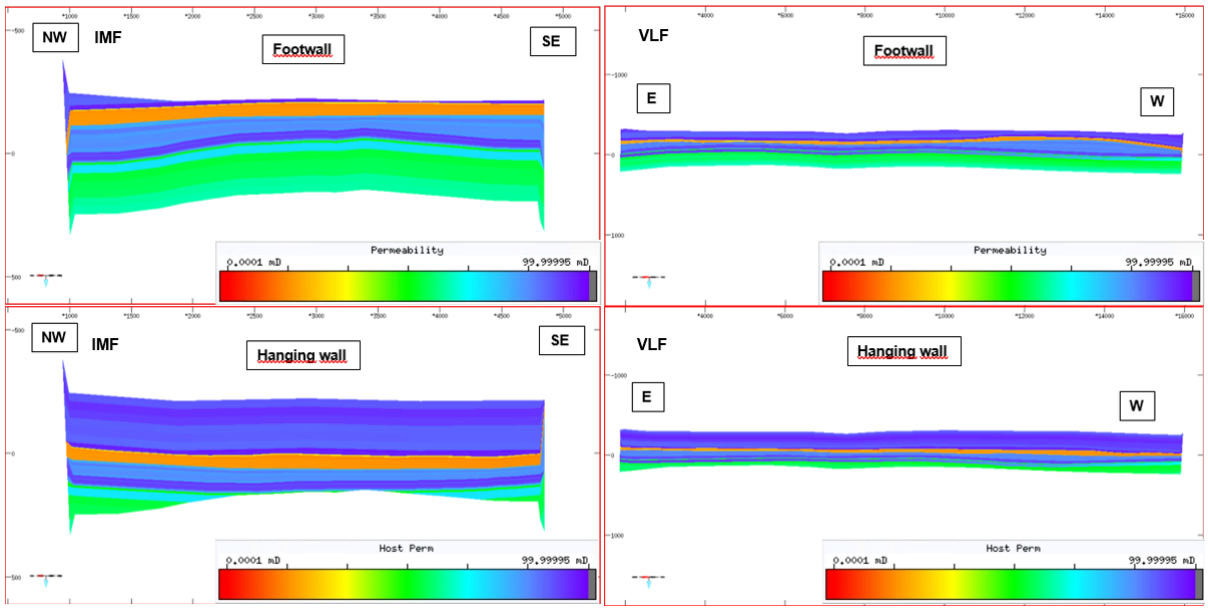

Fig. 13: Footwall and hanging wall permeability for the IMF (left) and the VLF (right)

Transmissibility multiplier

For the displayed transmissibility multiplier low values starting at 0 are displayed as red and high values ending at 1 are displayed as purple. Each increment represents an increase of 0.2 in the transmissibility multiplier value. In terms of colour this means: red to orange is (0.0-0.2), orange to yellow (0.2-0.4), yellow to green (0.4-0.6), green to light blue (0.6-0.8), and lastly, light blue to purple (0.8-1.0+),

Looking at the values calculated for the Il-Maghlaq Fault (fig. 14A) there is significant variation. Most of the values at the top and bottom of the fault are light blue to purple. This indicates a value greater than 0.6. Toward the middle section of the fault there is a zone of green to yellow in the upper half of the fault indicating values between 0.6 to 0.4. Further, there are three patches with red in the central part of the faults where the value is 0.

The Victoria Line Fault is a long fault segment (fig.14B), with a big variation of the transmissibility multiplier, both down dip and along strike. Starting at the eastern side of the fault we observe fairly high values at the top of the fault. The light blue to blue colour indicates values in the range between 0.6 to 0.8. There is a couple of small and thin patches of red toward the middle, sandwiched between two thin slivers of purple values. Underneath there is a thin sliver of yellow to orange colour indicating relatively low values in the range of 0.2 to 0.4, before the colour tuns purple blue to purple again giving a transmissibility

multiplier between 0.6 to 1.0. Moving along strike eastward there is a general decrease in the values predicted for the upper half of the fault. The top of the fault is slightly green and the lens in between the two thin purple areas is also turned green. Ther is also much bigger areas of red indicating bigger areas of low transmissibility multiplier values. In the lower half of the fault there looks to be a slight increase from mostly some light blue to almost only purple.

The Gozo fault has an overall high transmissibility multiplier (fig. 14C). In the western side the entire area is almost only purple, except for the red areas where the SSF were predicted with a thin sliver of light blue to slight greenish zone underneath. Moving along strike westward there is a noticeable decrease in the transmissivity multiplier value with the top being light blue to green in colour. In the lower half of the Gozo fault there is also a slight decrease in value as there is blueish tint to the colour.

The Pwales Fault has the same pattern as the other faults with a high transmissibility multiplier at the top and a higher at the bottom of the fault (fig.14D). In the middle there is a continuous red area with a low transmissibility multiplier.

The southern fault has a in general high transmissibility values, both the top and the bottom are purple indication a value of 1.0 (fig.14E). One thin zone of light blue stretches through the entire fault and a second thin zone underneath is fading from light blue to purple along strike east to west.

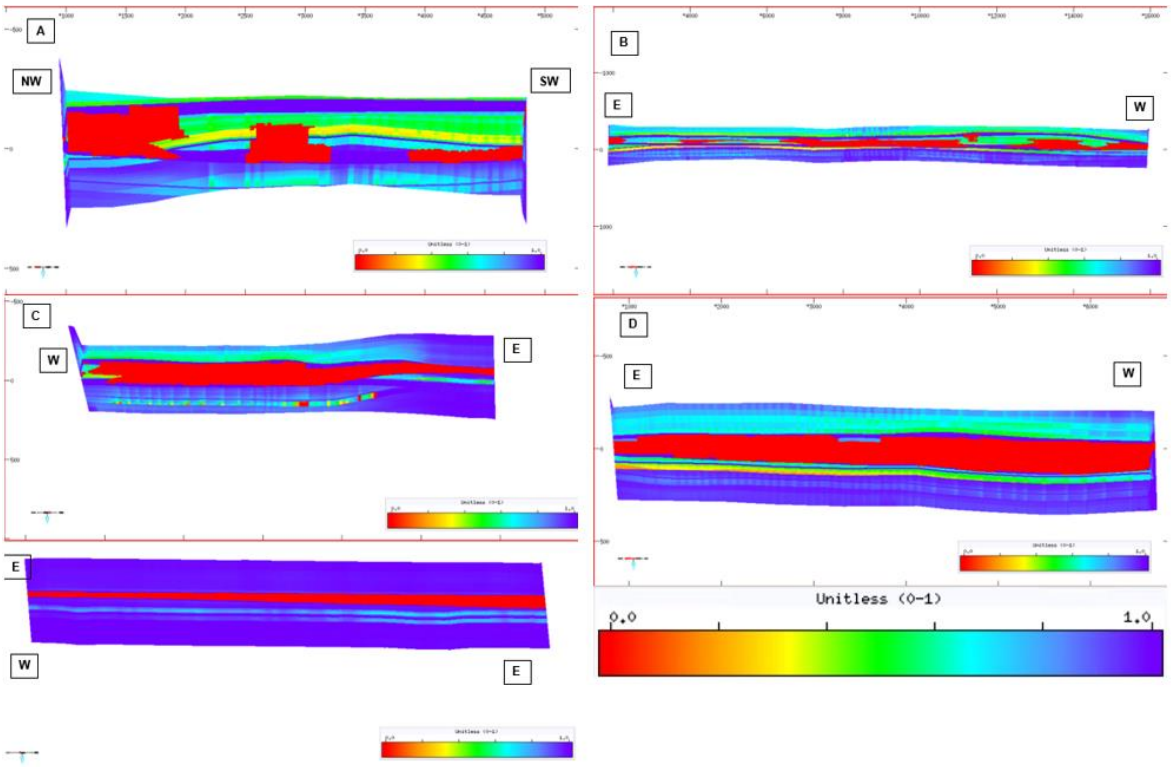

Fig. 14 transmissibility multipliers for the faults: A) IMF, B) VLF, C) Gozo Fault, D) Pwales Fault, and E) Southern Fault

4.2 Hydrogeology

4.2.1 GMS

The Il-Maghlaq Fault has a footwall and hanging wall consist of the two high permeable formations Lower Coralline Limestone and Upper Coralline Limestone juxtaposed against each other and thus given high values of hydraulic conductivity. The model is a simplified model so both sides of the fault consist of homogenous materials. From literature (Lotti et al., 2021) it was found that aquafer hydraulic conductivity could be in the range of 10-35 m/day, so a value of 10 m/day was tested for the model.

Model 1 – No fault zone

In the first model (fig 15) it was shown how the groundwater is calculated to be if the fault zone had no impact on the fluid flow. Here we see that the maximum water table is 0.8 meter above sea level and is decreasing linearly toward sea level at the coast. The model has three

observation wells close to the Il-Maghlaq fault, one located where the borehole 10085 is, the second is located directly beside the fault on the footwall side, and the third is located directly beside the fault zone in the hanging wall (see table 1 for values).

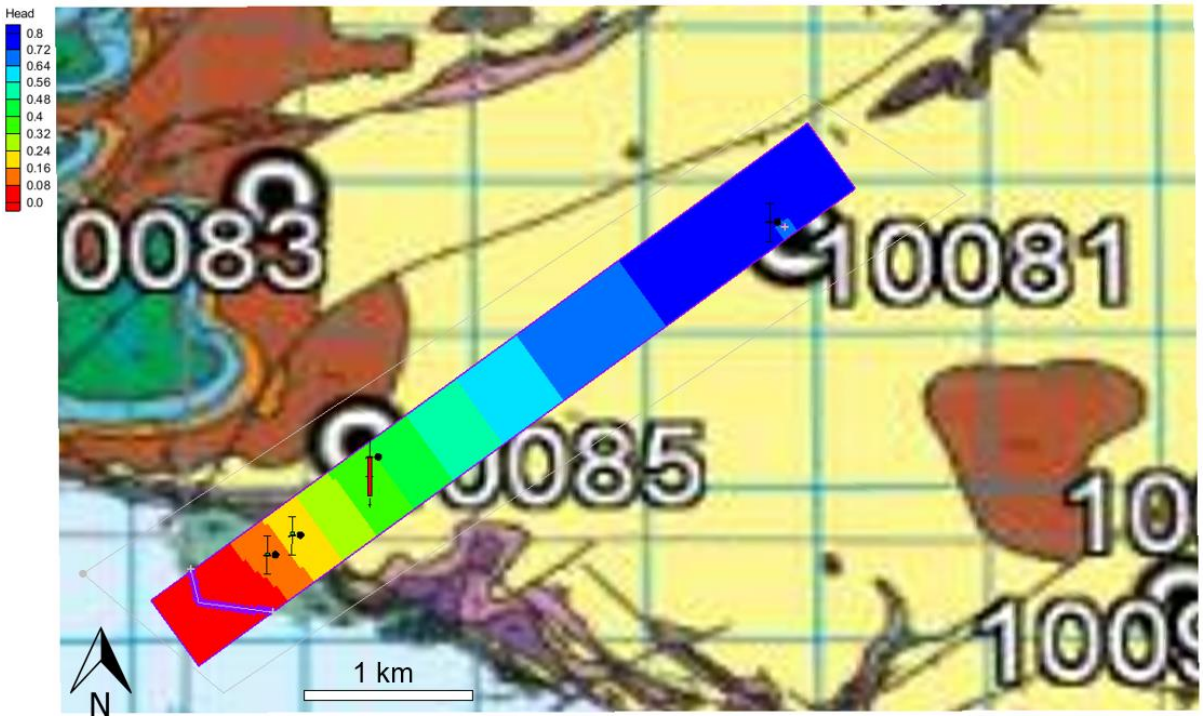

Fig. 15 visualisation of the calculated groundwater table with no impact of a fault zone

Model 2 – continuous fault zone

From the model in T7 it was confirmed that shale smear is located at the depth of the aquifer around sea level, thus it is possible to defend a lowering of the hydraulic conductivity by orders of magnitude. The second model show the area with a hydraulic conductivity lowered to 0.01 m/day across a fault zone roughly 15 m (fig.16). Here we clearly see that the water table is impacted and rising. It has also dropped severely on the hanging wall side and is rapidly decreasing to 0 m.a.s.l. The two observation wells on the footwall side of the fault shows the increase in water table on the aquifer side (see table 1).

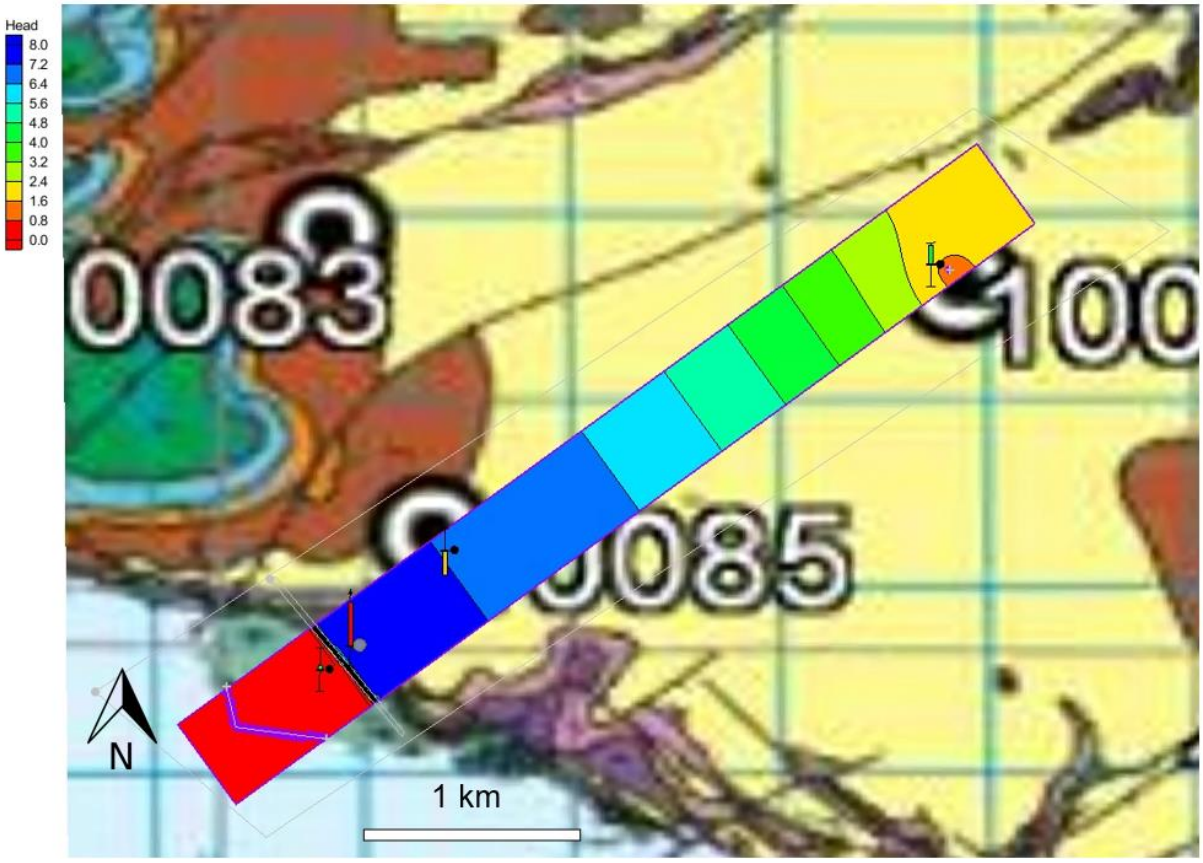

Fig. 16 visualisation of the calculated groundwater table with impact of a fault zone

Model 3 – thinned fault zone

The last model the fault zone was thinned toward the southern part, simulating a discontinued fault core (fig.17). Here we see a clear effect of how this allows the groundwater to migrate past the fault. The computed water table shows a higher water table at the northern end where the fault zone thickness is unchanged from model 2. Moving southward we observe a decrease in the water table toward the thinning. In the hanging wall the pattern is opposite. Here the water table has an increase toward the thinned area and decreasing toward the thicker fault zone (see table 1 for values). The water table for the rest of the modelled area has also decreased significantly. As we see a maximum water head of 3.6 m.a.s.l.

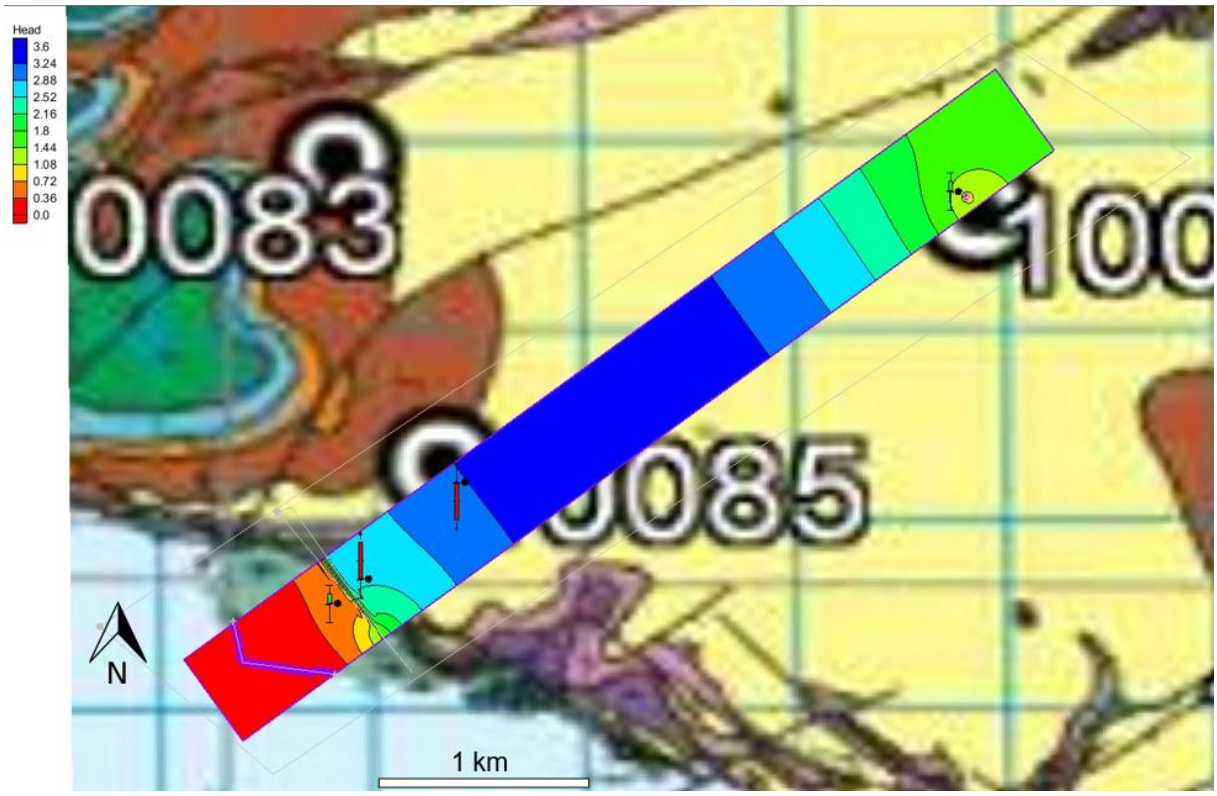

Fig. 17 visualisation of the calculated groundwater table with thinned fault zone

Table 1 Observed water head at the observation wells

Borehole / Model	Hanging wall water table	Footwall Water table	ID 10085 Water table	ID10081 Water table
1	0,8 m.a.s.l	1,2 m.a.s.l	2,1 m.a.s.l	1,2 m.a.s.l
2	0,2 m.a.s.l	7,3 m.a.s.l	7,2 m.a.s.l	1,7 m.a.s.l
3	0,5 m.a.s.l	2,6 m.a.s.l	3,2 m.a.s.l	1,3 m.a.s.l

5 Discussion

The aim of this study was to identify relationships in the modelled faults with regards to shale smear factor that may indicate sealing. By using assessing previously studied faults, groundwater and the modelled results we were able to identify some relationships between the sealing faults and those who are not. The first part in this discussion will be about the shale smear factor and how it impacts the predicted permeability- and transmissibility multiplier values. In the second part the effect of this will be discussed in the hydrogeological model, and lastly source of error and further studies.

5.1 SSF, Permeability and transmissibility multiplier

Correct interpretation of the shale smear factor is crucial for the model's ability to predict fault zone properties such as permeability and transmissibility multipliers. The critical threshold, also called cut-off value, for continuous shale smearing is an ongoing debate. A precise value is hard to estimate as shale smearing a complex process, but in generally taken as the throw divided by the thickness of the clay layer. For large seismic scale faults, a SSF ≤ 4 is considered as likely for continuous shale smear (Færseth, 2006). However, results from this modelling showed that this is not necessarily true. By looking at the Il-Maghlaq Fault we have found a reason to believe it may actually be higher. This fault is known to have a large throw and is one of the bounding faults of the Malta MSLA. This is linked with the wide zone of low permeability Blue Clay present along the fault plane. In fact, the fault surface consists of 40-86% Blue Clay, either through direct juxtaposition or through marl smear along the slip surface (Bonson et al., 2007).

In fig.12A and 14A, a SSF ≤ 4 is considered as the cut-off value for a continuous shale smear. However, the Il-Maghlaq Fault shows three patches with low fault zone permeability values and transmissibility multipliers close to zero. Surrounding these patches are areas with increased values, with the transmissibility multiplier being between 0.4 and 1.0. These values do not concur with a fault that is interpreted to be sealing. When investigating the SSF for the fault we see that these areas have values above 4, indicating that the cutoff value should be higher.

The same is observed for the permeability of the fault plane. All the fault planes have a similar permeability pattern of higher permeability in the uppermost part of the fault which is progressively getting lower down dip of the fault plane. This is because the algorithm uses the permeability of the juxtaposed formations to estimate fault zone permeability. This is also the case for areas where the SSF exceeds the cutoff value of 4. Here we get the same permeability range (0.1 – 10 mD) as if there were no fault rock. Only in areas where continues shale smear is assumed the predicted permeability is low and close to zero. This means that for a SSF ≥ 4 the model predicts a discontinuous shale smear, thus using the two juxtaposed formations to predict the fault zone permeability. This leads to a calculated value for permeability to be higher than expected in large parts of the Il-Maghlaq Fault.

The Pwales Costal Aquifer is in the Pwales Valley. This is a graben bounded aquifer in the Upper Coralline Limestone, which is bounded by the Manikata-Simar Fault in the north, the Pwales fault in the south, and the Blue Clay Formation underneath (Barbagli et al., 2021). The aquifers main source of freshwater recharge is from springs along the northern- and southern boundary (fig.18A) (Barbagli et al., 2021). From fig. 14 and 12 we can see that both the transmissibility multiplier and the fault zone permeability are fairly high, indicating that direct UCL-UCL juxtaposition is not baffling the fluid flow. Furthermore, the areas of the shale smear juxtaposed against the Blue Clay is calculated to have a SSF ≥ 5, indicating a discontinuous shale smear allowing fluids to migrate through the fault and into the aquifer (fig.18B).

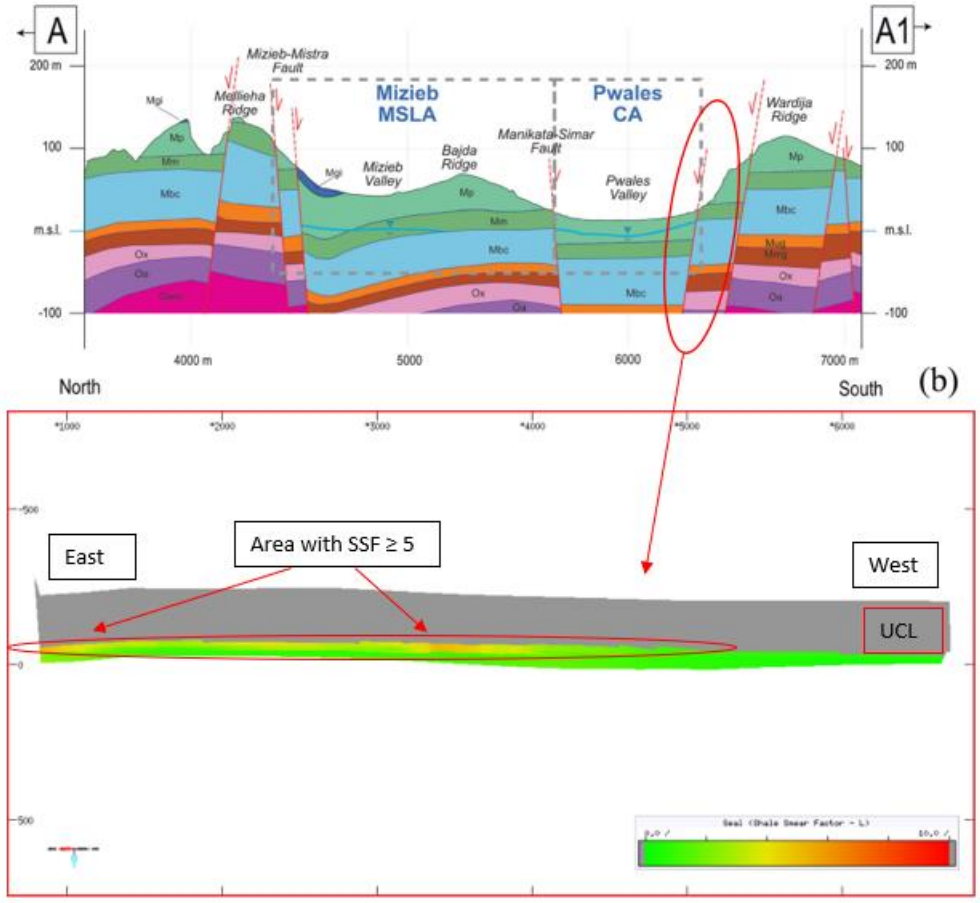

Fig. 18 A) cross-section of Pwales fault, modified form Barbagli (2021). B) SSF of Pwales fault showing only areas juxtaposed against the UCL

The shale smear factor equation only uses two variables; throw and clay layer thickness. So, for the fault with larger throw such as the Il-Maghlaq Fault and the Victoria Line Fault (fig 13) it is crucial that the shaly/clay layer has sufficient thickness. For instance, a shale smear factor of less than 4 for the Il-Maghlaq fault the Blue Clay must have been 50 m thick at the time of faulting and for a factor less than 5 the same layer must be at least 40 m thick. This concurs with the thickness of the Blue Clay in the model. The Blue Clay is thickest in the northern part of the Il-Maghlaq Fault being up to 55 m thick, while in the southern part it is only 40 m (fig. 13). Therefore, the area surrounding large scale faults on the Maltese Island should be handled with care to best exploit the water resources on the island.

Using these observations, we propose the shale smear critical threshold value for this case study should be increased. Specifically, a SSF ≤ 5 is likely to produce continuous shale smearing for fault on the Maltese Islands.

Considering a cutoff value of 5 for the same faults (fig.19) we see a notable change in the area with predicted low permeability and transmissibility multiplier compared to the cutoff value set to 4 (fig. 14A). For the Il-Maghlaq Fault, a continuous smear is predicted across the length of the fault. Hence, this fault is interpreted to be sealing.

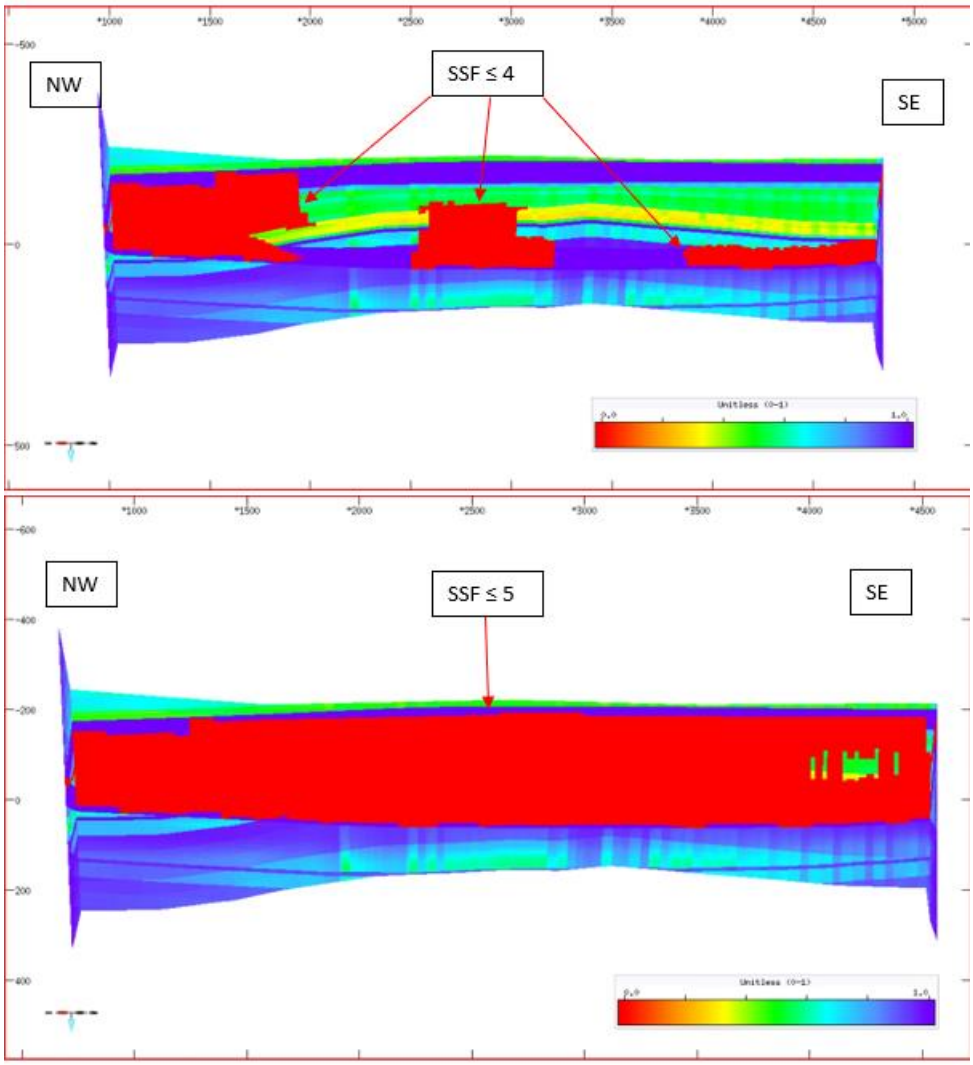

Fig. 19: difference in fault rock continuity predicted with SSF ≤ 4 (top picture) and SSF ≤ 5 (picture below)

The Victoria Line Fault is a large graben bounding fault, and may be interpreted as acting as a seal or baffle. However, it has been shown to pose no impact on the Malta MSLA (Barbagli et al., 2021; Lotti et al., 2021). Hence, an important question to answer is why the Victoria Line Fault does not act as a bounding fault in the same way as the Il-Maghlaq Fault? The answer may be as simple as there isn't a large enough throw so the shale smear does not reaches down to the depth of the aquifer, especially on the eastern side of the fault, as shown in fig.20. This means that it is only Lower Coralline Limestone juxtaposed against each other, which from the transmissibility multiplier calculation will increase the fluid flow rather than baffling

it. High SSF is predicted on the eastern side of the Victoria Line Fault, however, this may not necessarily be accurate. In that region, the Blue Clay is eroded and absent from the surface. The thickness of the Blue Clay poses a huge source of error for the model, as no subsurface data is available, and it is no way of knowing precisely the thickness or throw.

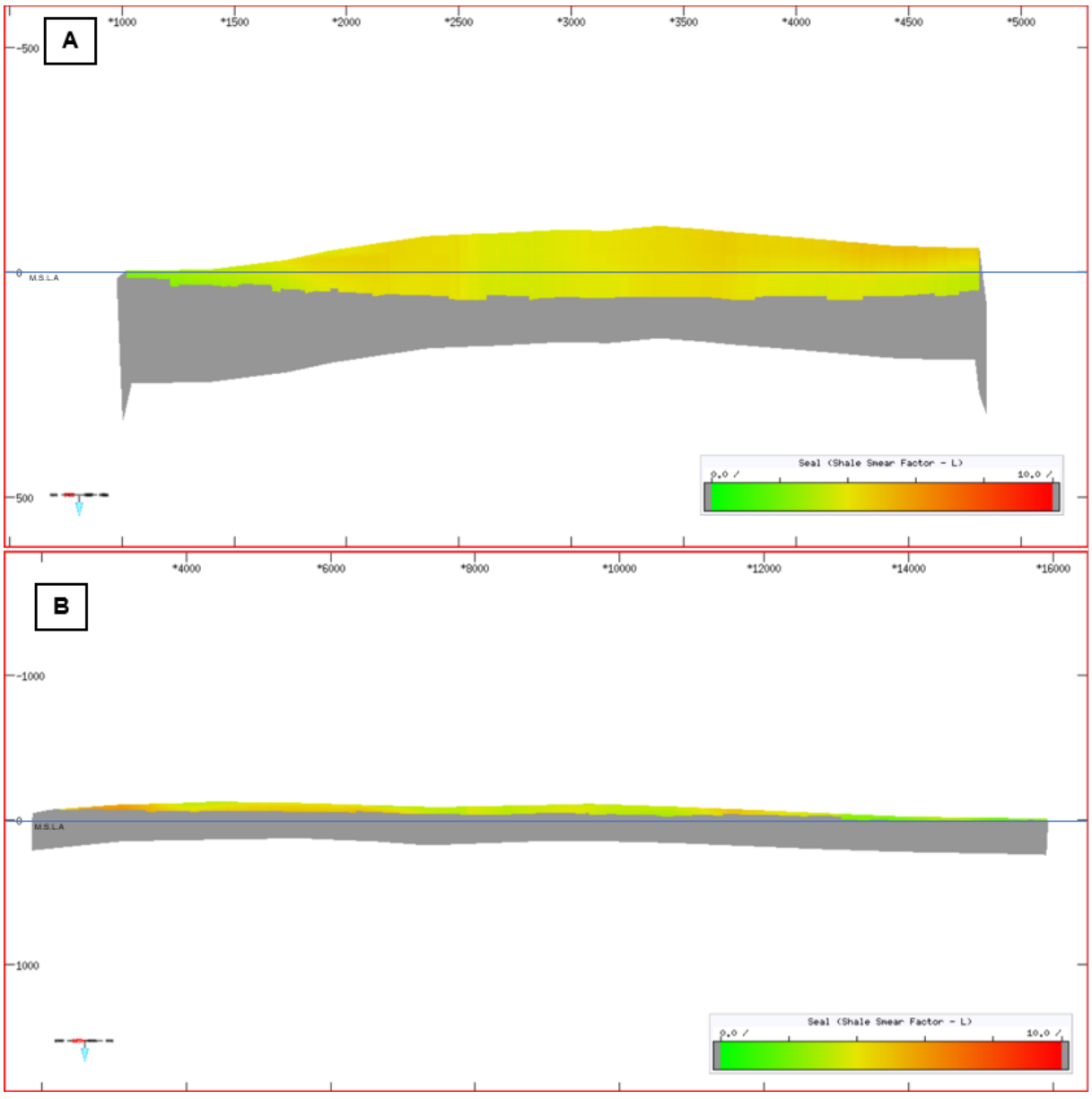

Fig. 20: difference in area predicted for LCL to have shale smear. the faults shown are A) IMF and B) VLF. The blue line represents sea level.

With the assumption of no shale smear at the depth of the Malta MSLA, other faults have to be investigated for understanding of across fault fluid migration as there is no available well data on the hanging wall side of the Victoria Line Fault. Unfortunately, there is no

comparable faults south of the Victoria Line Fault. However, it is possible to look at fault with available well data and low throw, such as the fault I have called the Southern Fault. Here we also see a fault that is not impacted by the shale smear. From literature, LCL-LCL juxtaposition in faults of low displacement should give an intermediate permeability and transmissibility multiplier as it is prone to form cataclasites and cementation (Michie et al., 2018). This is also the case for the Southern Fault (fig.10E). Well data from borehole ID 10366 and 10353 we see that there is a slight decrease from 1,8 m.a.s.l to 0,4 m.s.l.a, indicating a slight baffle. However, this might be influenced by other faults close by, and the distance between the wells.

The Gozo Fault is also a fault showing promising attributes to be a sealing fault for the Ghajnsielem PA, however, little groundwater data is available to confirm this. The area where UCL is juxtaposed against the shale smear is wide and the values are low. This is a good signs of fluid sealing and can be an interesting fault to research closer.

5.2 Hydrogeological model

In general, the Malta MSLA has a relatively similar water table across the entire aquifer. The areas in southern Malta, where most of the well data provided are located, is lacking the Blue Clay Formation due to erosion (Pedley et al., 1976). Combined with only faults of low throw has resulted in faults with relatively little impact on the groundwater table. This is also visible on the groundwater data provided, as it is only small variations in the groundwater across large areas. However, one borehole shows a significant change in water table height. This is the borehole with ID 10085, located just west of the Il-Maghlaq Fault, showing an increase in water table height of up to eight times the normal water table across the island, which may indicate that the fault is sealing. However, there is no bore hole data in the hanging wall proving a significant drop in water table. Since this is the fault with the best groundwater data it was chosen to show three different scenarios: a homogenic with no influence of a fault rock, a model with continuous fault rock, and a discontinuous fault roc.

The first model with no influence from the fault rock. The entire modelled area was set to have a hydraulic conductivity if 10 m/day, which is kept throughout all models. Here the groundwater showed a linear decrease toward the sea, which is expected of an aquifer in a

homogenous material. This can be used as an analogue to low-throw faults across the Malta MSLA, where the Lower Coralline Limestone is self-juxtaposed.

When implementing the fault zone permeability using calculated values from T7, we see that there is a change in the groundwater. The first noticeable difference is a decrease from 10 m/day to 0.01 m/day, which caused an increase in water table from 0.2 to 9.0 m. This decrease in hydraulic conductivity also led to an increase in the groundwater further away from the coast. Around the bore hole ID 10081 there is almost a 2 m increase of groundwater, which does not correlate with observed water head from the borehole data. However, this may be due to the by the model being a steady-state model, so the amount of water in the system is the same throughout the simulation. Meaning no water will escape through the boundaries of the model area. Since the fault zone acts as a barrier the amount of water has effectively less area to be stored, thus increasing the water table further inland. While in reality, the water would have a larger area to cover. The overall estimation of this model honours the observed water table near the Il-Maghlaq Fault, thus supporting our claim that this fault is a bounding fault for the Malta MSLA.

In the last groundwater model (fig.17), we see the importance of a continuous fault core. The thickness of the fault core in the southern section of the fault was severely thinned compared to the northern side, but the same hydraulic conductivity was used. Here we see that the fault now longer is predicted to act completely as a barrier, but rather a baffle as it is predicted to leak from this zone. This is an important result as it may show why the Victoria Line Fault is bounding the Malta MSLA. As aforementioned, the Victora Line Fault show a thinning in the Blue Clay on the eastern side of the fault, causing an increase in the SSF, while on the western side the Blue Clay is thicker meaning the fault may be sealing in this area (fig.20).

It is important to remember that this hydrogeological model us highly simplified as the main goal of the thesis is to do a structural analysis of the fault. Further studies, where fault data from this thesis could be implemented needs to be done for a more realistic groundwater model.

5.3 Source of error and further studies

As previously mentioned, membrane seals in siliciclastic rocks have been researched for decades, and the algorithm for SSF has been used and tested in the industry for years after the

algorithm was developed. These algorithms have proven to work and can be relied upon. However, this is not the case for the membrane seal in carbonates. Few publications have focussed illustrating whether the SSF can be accurately and reliably used in carbonates. The algorithm used in T7 bases its calculations of fault zone permeability on host rock permeability values (Michie et al., 2021). Further, there is no data on the porosity and permeability of the Blue Clay Formation, it is just assumed set to be close to zero. The Blue Clay (a marl) is also assumed to deform in the same way as siliciclastic rocks, as it uses similar equation to calculate the area of shale smear. However, the model seems to produce an accurate representation of the two islands with regards to field studies performed. To further strengthen this, more studies have to be conducted on the Blue Clay as it quite possibly is the key formation for sealing faults on the islands.

6 Conclusion

The overall goal of this thesis was to improve understand fault seal in carbonate sequences. The main objective was to create and populate a geocellular model of the Maltese islands, which was used to analyse fault seal potential across the islands. Shale smear factor, permeability, and transmissibility multipliers were calculated for each of the faults. For faults with a low throw had a thin zone with low shale smear factors were predicted. However, because of the low throw these faults were not able to create a trap that could impact the aquifer. Faults with large throw had a wide zone of shale smear predicted of a wide range of SSF values. By using well data provided close to the Il-Maghlaq Fault and comparing it to the Pwales Fault we were able to establish that a SSF ≤ 5 is likely to produce a continuous shale smear. However, it is not a sufficient number of faults with this order of throw in the two islands to conclude this, so more research needs to be done

By assuming a continuous shale smear we were able to reproduce a groundwater model similar to what is observed in the Malta MSLA. We suggest more detailed models should be made with regards to groundwater exploiting.

If this is applicable to other area such as the Cromer Knoll Formation is not known. However, a good starting point is to assess well data of the formation to establish the permeability of the undeformed host rock. Then use seismic data to calculate the thickness of the formation and the throw distance of the faults. Knowing what SSF we may need to use for marls is crucial. We could reduce uncertainty when assessing CO_2-storage sites like Smeaheia by using accurate cutoff values and may be able to apply the cutoff value of 5 to Smeaheia.

References

Agosta, F., Alessandroni, M., Antonellini, M., Tondi, E., & Giorgioni, M. (2010). From fractures to flow: A field-based quantitative analysis of an outcropping carbonate reservoir. *Tectonophysics*, *490*(3–4). https://doi.org/10.1016/j.tecto.2010.05.005

Agosta, F., Prasad, M., & Aydin, A. (2007). Physical properties of carbonate fault rocks, fucino basin (Central Italy): Implications for fault seal in platform carbonates. *Geofluids*, *7*(1). https://doi.org/10.1111/j.1468-8123.2006.00158.x

Andre, B. J., & Rajaram, H. (2005). Dissolution of limestone fractures by cooling waters: Early development of hypogene karst systems. *Water Resources Research*, *41*(1). https://doi.org/10.1029/2004WR003331

Argnani, A. (1990). The strait of sicily rift zone: Foreland deformation related to the evolution of a back-arc basin. *Journal of Geodynamics*, *12*(2–4). https://doi.org/10.1016/0264-3707(90)90028-S

Barbagli, A., Guastaldi, E., Conti, P., Giannuzzi, M., Borsi, I., Lotti, F., Basile, P., Favaro, L., Mallia, A., Xuereb, R., Schembri, M., Mamo, J. A., & Sapiano, M. (2021). Geological and hydrogeological reconstruction of the main aquifers of the Maltese islands. *Hydrogeology Journal*, *29*(8). https://doi.org/10.1007/s10040-021-02406-z

Bastesen, E., & Braathen, A. (2010). Extensional faults in fine grained carbonates - analysis of fault core lithology and thickness-displacement relationships. *Journal of Structural Geology*, *32*(11). https://doi.org/10.1016/j.jsg.2010.09.008

Bense, V. F., Gleeson, T., Loveless, S. E., Bour, O., & Scibek, J. (2013). Fault zone hydrogeology. In *Earth-Science Reviews* (Vol. 127). https://doi.org/10.1016/j.earscirev.2013.09.008

Billi, A. (2005). Attributes and influence on fluid flow of fractures in foreland carbonates of southern Italy. *Journal of Structural Geology*, *27*(9). https://doi.org/10.1016/j.jsg.2005.05.001

Billi, A., Salvini, F., & Storti, F. (2003). The damage zone-fault core transition in carbonate rocks: Implications for fault growth, structure and permeability. *Journal of Structural Geology*, *25*(11). https://doi.org/10.1016/S0191-8141(03)00037-3

Billi, A., Valle, A., Brilli, M., Faccenna, C., & Funiciello, R. (2007). Fracture-controlled fluid circulation and dissolutional weathering in sinkhole-prone carbonate rocks from central Italy. *Journal of Structural Geology*, *29*(3). https://doi.org/10.1016/j.jsg.2006.09.008

Bonson, C. G., Childs, C., Walsh, J. J., Schöpfer, M. P. J., & Carboni, V. (2007). Geometric and kinematic controls on the internal structure of a large normal fault in massive

limestones: The Maghlaq Fault, Malta. *Journal of Structural Geology*, *29*(2). https://doi.org/10.1016/j.jsg.2006.06.016

Caine, J. S., Evans, J. P., & Forster, C. B. (1996). Fault zone architecture and permeability structure. *Geology*, *24*(11). https://doi.org/10.1130/0091-7613(1996)024<1025:FZAAPS>2.3.CO;2

Celico, F., Petrella, E., & Celico, P. (2006). Hydrogeological behaviour of some fault zones in a carbonate aquifer of Southern Italy: An experimentally based model. *Terra Nova*, *18*(5). https://doi.org/10.1111/j.1365-3121.2006.00694.x

Chester, F. M., & Logan, J. M. (1986). Implications for mechanical properties of brittle faults from observations of the Punchbowl fault zone, California. *Pure and Applied Geophysics PAGEOPH*, *124*(1–2). https://doi.org/10.1007/BF00875720

Cooke, A. P., Fisher, Q. J., Michie, E. A. H., & Yielding, G. (2018). Investigating the controls on fault rock distribution in normal faulted shallow burial limestones, Malta, and the implications for fluid flow. *Journal of Structural Geology*, *114*. https://doi.org/10.1016/j.jsg.2018.05.024

Cooke, A. P., Fisher, Q. J., Michie, E. A. H., & Yielding, G. (2019). Permeability of carbonate fault rocks: A case study from malta. *Petroleum Geoscience*, *26*(3). https://doi.org/10.1144/petgeo2019-055

Dart, C. J., Bosence, D. W. J., & McClay, K. R. (1993). Stratigraphy and structure of the Maltese Graben system. *Journal - Geological Society (London)*, *150*(6). https://doi.org/10.1144/gsjgs.150.6.1153

Færseth, R. B. (2006). Shale smear along large faults: Continuity of smear and the fault seal capacity. *Journal of the Geological Society*, *163*(5). https://doi.org/10.1144/0016-76492005-162

Faulkner, D. R., Jackson, C. A. L., Lunn, R. J., Schlische, R. W., Shipton, Z. K., Wibberley, C. A. J., & Withjack, M. O. (2010). A review of recent developments concerning the structure, mechanics and fluid flow properties of fault zones. In *Journal of Structural Geology* (Vol. 32, Issue 11). https://doi.org/10.1016/j.jsg.2010.06.009

Ferrill, D. A., & Morris, A. P. (2008). Fault zone deformation controlled by carbonate mechanical stratigraphy, Balcones fault system, Texas. *American Association of Petroleum Geologists Bulletin*, *92*(3). https://doi.org/10.1306/10290707066

Ferrill, D. A., Morris, A. P., McGinnis, R. N., Smart, K. J., Wigginton, S. S., & Hill, N. J. (2017). Mechanical stratigraphy and normal faulting. In *Journal of Structural Geology* (Vol. 94). https://doi.org/10.1016/j.jsg.2016.11.010

Fisher, Q. J., & Knipe, R. J. (1998). Fault sealing processes in siliciclastic sediments. *Geological Society Special Publication*, *147*. https://doi.org/10.1144/GSL.SP.1998.147.01.08

Fulljames, J. R., Zijerveld, L. J. J., & Franssen, R. C. M. W. (1997). Fault seal processes: systematic analysis of fault seals over geological and production time scales. *Norwegian Petroleum Society Special Publications*, *7*(C). https://doi.org/10.1016/S0928-8937(97)80006-9

Gabrielsen, R. H., Skurtveit, E., & Faleide, J. I. (2020). Caprock integrity of the draupne formation, ling depression, north sea, norway. *Norwegian Journal of Geology*, *100*(4). https://doi.org/10.17850/njg100-4-2

Hausegger, S., Kurz, W., Rabitsch, R., Kiechl, E., & Brosch, F. J. (2010). Analysis of the internal structure of a carbonate damage zone: Implications for the mechanisms of fault breccia formation and fluid flow. *Journal of Structural Geology*, *32*(9). https://doi.org/10.1016/j.jsg.2009.04.014

John, C. M., Mutti, M., & Adatte, T. (2003). Mixed carbonate-siliciclastic record on the North African margin (Malta) - Coupling of weathering processes and mid Miocene climate. *Bulletin of the Geological Society of America*, *115*(2). https://doi.org/10.1130/0016-7606(2003)115<0217:MCSROT>2.0.CO;2

Kim, Y. S., Peacock, D. C. P., & Sanderson, D. J. (2004). Fault damage zones. *Journal of Structural Geology*, *26*(3). https://doi.org/10.1016/j.jsg.2003.08.002

Knipe, R. J., Fisher, Q. J., Jones, G., Clennell, M. R., Farmer, A. B., Harrison, A., Kidd, B., Mcallister, E., Porter, J. R., & White, E. A. (1997). Fault seal analysis: successful methodologies, application and future directions. *Norwegian Petroleum Society Special Publications*, *7*(C). https://doi.org/10.1016/S0928-8937(97)80004-5

Lauritsen, H., Kassold, S., Meneguolo, R., & Furre, A. (2018). Assessing potential influence of nearby hydrocarbon production on CO2 storage at Smeaheia. *5th CO2 Geological Storage Workshop*, *2018-November*. https://doi.org/10.3997/2214-4609.201802970

Lehner, F. K., & Pilaar, W. F. (1997). The emplacement of clay smears in synsedimentary normal faults: inferences from field observations near Frechen, Germany. *Norwegian Petroleum Society Special Publications*, *7*(C). https://doi.org/10.1016/S0928-8937(97)80005-7

Lindsay, N. G., Murphy, F. C., Walsh, J. J., & Watterson, J. (1993). Outcrop studies of shale smears on fault surfaces. *The Geological Modelling of Hydrocarbon Reservoirs and Outcrop Analogues*.

Little, M. G., & Jackson, R. B. (2010). Potential impacts of leakage from deep CO2 geosequestration on overlying freshwater aquifers. *Environmental Science and Technology*, *44*(23). https://doi.org/10.1021/es102235w

Lotti, F., Borsi, I., Guastaldi, E., Barbagli, A., Basile, P., Favaro, L., Mallia, A., Xuereb, R., Schembri, M., Mamo, J. A., & Sapiano, M. (2021). Numerically enhanced conceptual modelling (NECoM) applied to the Malta Mean Sea Level Aquifer. *Hydrogeology Journal*. https://doi.org/10.1007/s10040-021-02330-2

Manzocchi, T., Walsh, J. J., Nell, P., & Yielding, G. (1999). Fault transmissibility multipliers for flow simulation models. *Petroleum Geoscience*, *5*(1). https://doi.org/10.1144/petgeo.5.1.53

Matonti, C., Lamarche, J., Guglielmi, Y., & Marié, L. (2012). Structural and petrophysical characterization of mixed conduit/seal fault zones in carbonates: Example from the Castellas fault (SE France). *Journal of Structural Geology*, *39*. https://doi.org/10.1016/j.jsg.2012.03.003

Micarelli, L., Benedicto, A., & Wibberley, C. A. J. (2006). Structural evolution and permeability of normal fault zones in highly porous carbonate rocks. *Journal of Structural Geology*, *28*(7). https://doi.org/10.1016/j.jsg.2006.03.036

Michie, E. A. H., Cooke, A. P., Kaminskaite, I., Stead, J. C., Plenderleith, G. E., Tobiss, S. D., Fisher, Q. J., Yielding, G., & Freeman, B. (2020). Key controls on the hydraulic properties of fault rocks in carbonates. *Petroleum Geoscience*. https://doi.org/10.1144/petgeo2020-034

Michie, E. A. H., Haines, T. J., Healy, D., Neilson, J. E., Timms, N. E., & Wibberley, C. A. J. (2014). Influence of carbonate facies on fault zone architecture. *Journal of Structural Geology*, *65*. https://doi.org/10.1016/j.jsg.2014.04.007

Michie, E. A. H., Kaminskaite, I., Cooke, A. P., Fisher, Q. J., Yielding, G., & Tobiss, S. D. (2021). Along-strike permeability variation in carbonate-hosted fault zones. *Journal of Structural Geology*, *142*. https://doi.org/10.1016/j.jsg.2020.104236

Michie, E. A. H., Yielding, G., & Fisher, Q. J. (2018). Predicting transmissibilities of carbonate-hosted fault zones. In *Geological Society Special Publication* (Vol. 459, Issue 1). https://doi.org/10.1144/SP459.9

Mullis, A. M. (1993). Determination of the rate-limiting mechanism for quartz pressure dissolution. *Geochimica et Cosmochimica Acta*, *57*(7). https://doi.org/10.1016/0016-7037(93)90009-L

Mulrooney, M. J., Osmond, J. L., Skurtveit, E., Faleide, J. I., & Braathen, A. (2020). Structural analysis of the Smeaheia fault block, a potential CO2 storage site, northern Horda Platform, North Sea. *Marine and Petroleum Geology*, *121*. https://doi.org/10.1016/j.marpetgeo.2020.104598

Pedley, H. M., House, M. R., & Waugh, B. (1976). The geology of Malta and Gozo. *Proceedings of the Geologists' Association*, *87*(3). https://doi.org/10.1016/S0016-7878(76)80005-3

Sibson, R. H. (1977). Fault rocks and fault mechanisms. *Journal of the Geological Society*, *133*(3). https://doi.org/10.1144/gsjgs.133.3.0191

Solum, J. G., & Huisman, B. A. H. (2017). Toward the creation of models to predict static and dynamic fault-seal potential in carbonates. *Petroleum Geoscience*, *23*(1). https://doi.org/10.1144/petgeo2016-044

Stuart, M. E., Maurice, L., Heaton, T. H. E., Sapiano, M., Micallef Sultana, M., Gooddy, D. C., & Chilton, P. J. (2010). Groundwater residence time and movement in the Maltese islands - A geochemical approach. *Applied Geochemistry*, *25*(5). https://doi.org/10.1016/j.apgeochem.2009.12.010

Tondi, E. (2007). Nucleation, development and petrophysical properties of faults in carbonate grainstones: Evidence from the San Vito Lo Capo peninsula (Sicily, Italy). *Journal of Structural Geology*, *29*(4). https://doi.org/10.1016/j.jsg.2006.11.006

Vrolijk, P. J., Urai, J. L., & Kettermann, M. (2016). Clay smear: Review of mechanisms and applications. In *Journal of Structural Geology* (Vol. 86). https://doi.org/10.1016/j.jsg.2015.09.006

Yielding, G., Bretan, P., & Freeman, B. (2010). Fault seal calibration: A brief review. *Geological Society Special Publication*, *347*. https://doi.org/10.1144/SP347.14

Yielding, G., Freeman, B., & Needham, D. T. (1997). Quantitative fault seal prediction. *AAPG Bulletin*, *81*(6). https://doi.org/10.1306/522b498d-1727-11d7-8645000102c1865d

Zheng, L., Apps, J. A., Zhang, Y., Xu, T., & Birkholzer, J. T. (2009). On mobilization of lead and arsenic in groundwater in response to CO2 leakage from deep geological storage. *Chemical Geology*, *268*(3–4). https://doi.org/10.1016/j.chemgeo.2009.09.007

Zhou, Y., & Li, W. (2011). A review of regional groundwater flow modeling. *Geoscience Frontiers*, *2*(2). https://doi.org/10.1016/j.gsf.2011.03.003

Appendix A

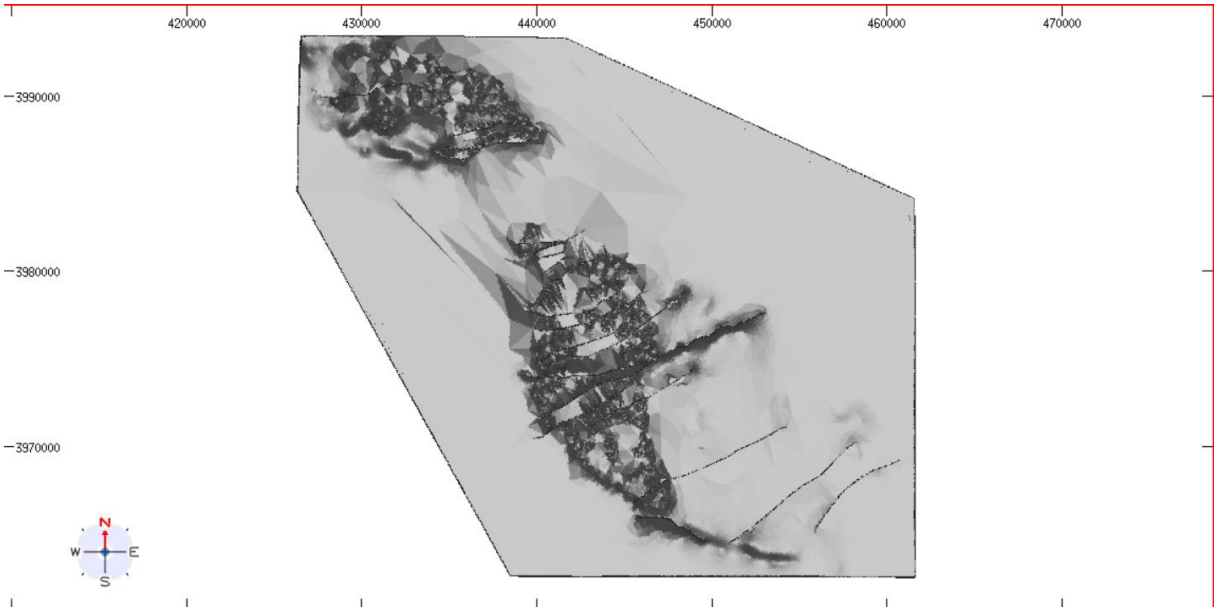

Fig. 21 Overview of the geocellular model

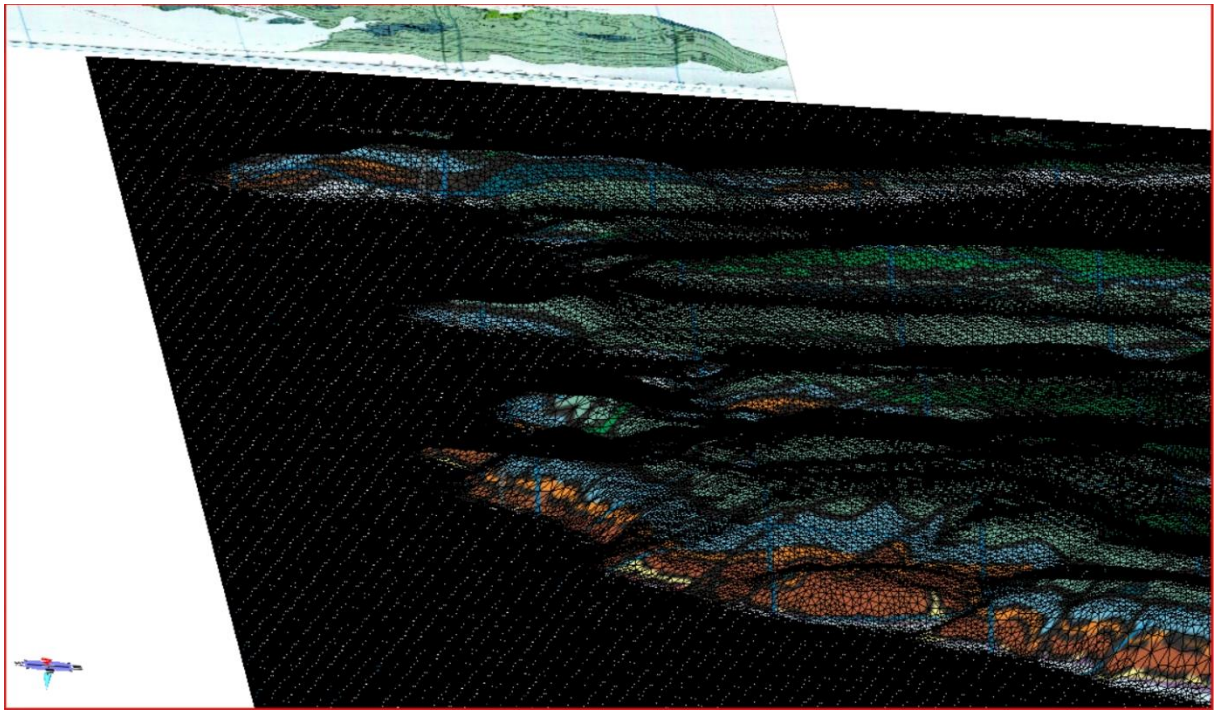

Fig. 22 shows how DEM and futures on the geological map was fitted

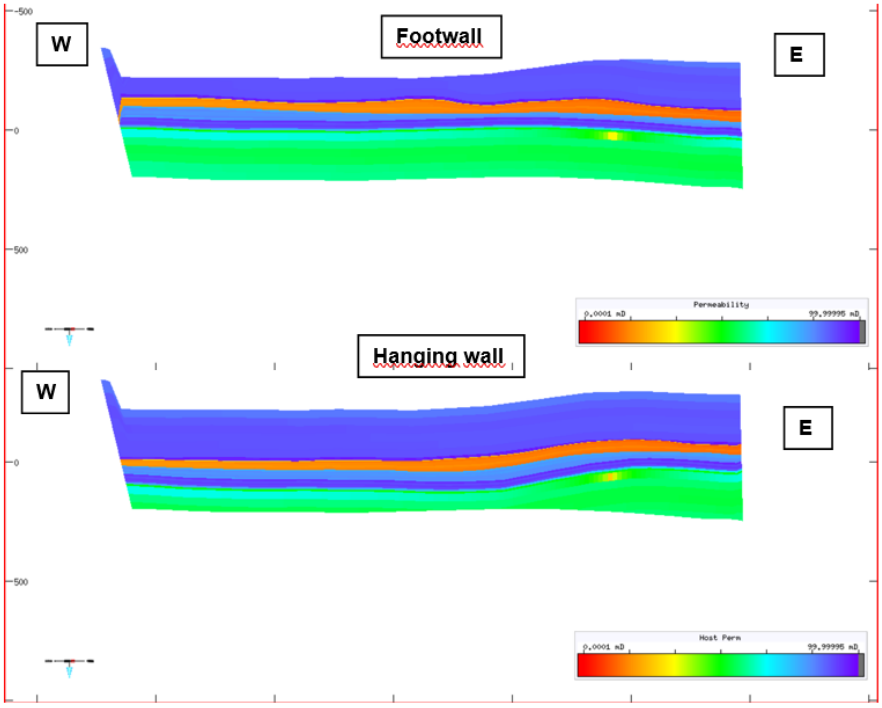

Fig. 23: Footwall and hanging wall permeability for the Gozo Fault

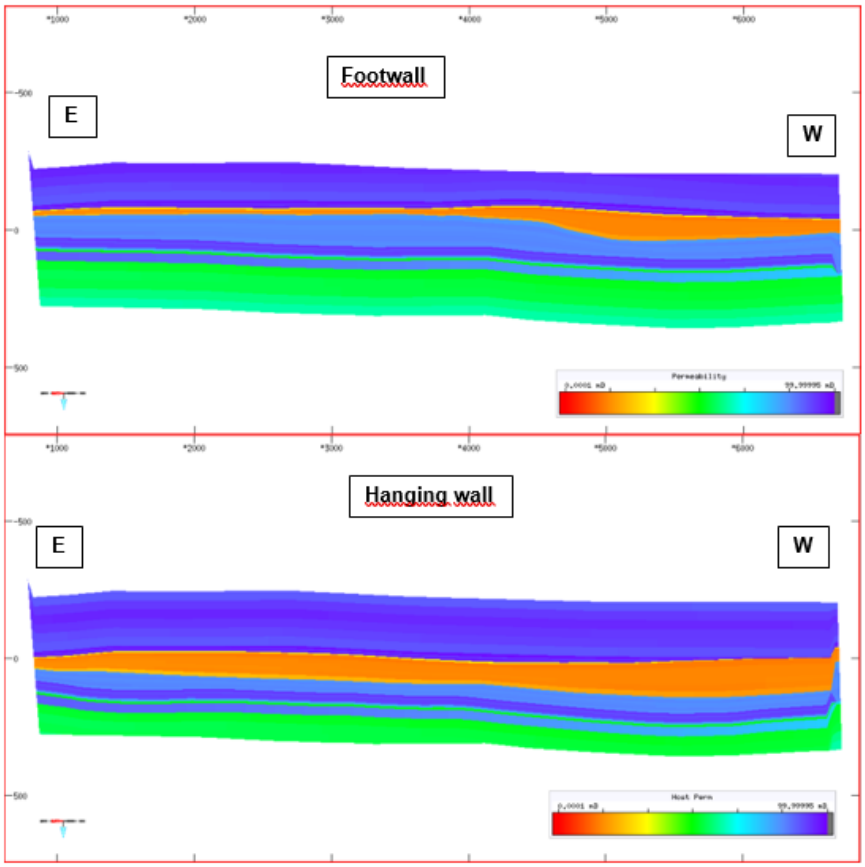

Fig. 24 Footwall and hanging wall permeability for the Pwales Fault

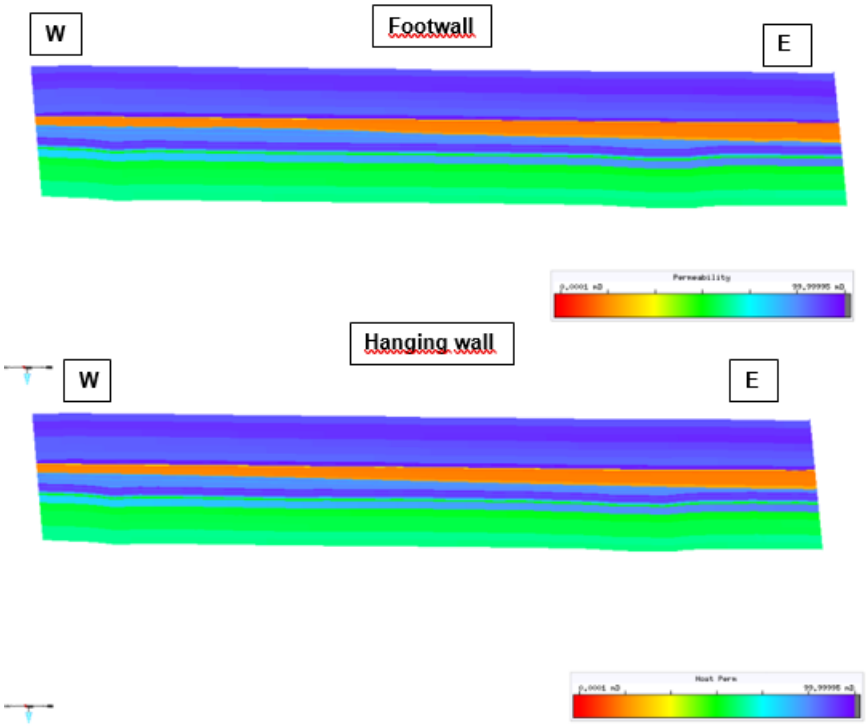

Fig. 25 Footwall and hanging wall Permeability for Southern Fault

Appendix B

Table 2: average water table for the individual boreholes form 1. January to 1. April

Borehole ID	Water table (m.s.l.a)
10035	2.1
10049	1.6
10058	1.9
10076	1,6
10078	1.8
10081	0.7
10083	2.0
10085	8.5
10089	1.5
10095	1.9
10097	1.2
10247	1.4
10259	2.3
10353	0.5
10366	1.8
10371	2,0